J. theor. Biol. (2003) **220,** 419–455
doi:10.1006/jtbi.2003.3115, available online at http://www.idealibrary.com on IDEAL®

Application of a Single-solute Non-steady-state Phloem Model to the Study of Long-distance Assimilate Transport

MATTHEW V. THOMPSON*† AND N. MICHELE HOLBROOK†

†*Biological Laboratories* 3113, 16 *Divinity Avenue*, *Department of Organismic and Evolutionary Biology*, *Harvard University*, *Cambridge*, *MA* 02138, *U.S.A.*

(*Received on* 26 *November* 2001, *Accepted in revised form on* 13 *June* 2002)

A mass-balanced, finite-difference solution to Münch's osmotically generated pressure-flow hypothesis is developed for the study of non-steady-state sucrose transport in the phloem tissue of plants. Major improvements over previous modeling efforts are the inclusion of wall elasticity, nonlinear functions of viscosity and solute potential, an enhanced calculation of sieve pore resistance, and the introduction of a slope-limiting total variation diminishing method for determining the concentration of sucrose at node boundaries. The numerical properties of the model are discussed, as is the history of the modeling of pressure-driven phloem transport. Idealized results are presented for a sharp, fast-moving concentration front, and the effect of changing sieve tube length on the transport of sucrose in both the steady-state and non-steady-state cases is examined. Most of the resistance to transport is found to be axial, rather than radial (via membrane transport), and most of the axial resistance is due to the sieve plates. Because of the sieve plates, sieve tube elasticity does not provide a significant enhancement to conductivity at high pressure, as previously suspected. The transit time of sucrose through a sieve tube is found to be inversely proportional to the square of the sieve tube's length; following that observation, it is suggested that 20 1-m-long sieve tubes could transport sucrose 20 times faster than a single 20 m sieve tube. Short sieve tubes would be highly sensitive to differentials between loading and unloading rate, and would require close cooperation with adjacent companion cells for proper function.
© 2003 Elsevier Science Ltd. All rights reserved.

1. Introduction

Water, nutrients, and other materials are transported within plants via two parallel cellular conduit systems, each internally highly redundant. These are the xylem, responsible for the transport of water and nutrients from the soil to the leaf, and the phloem, responsible for the transport of photosynthates, amino acids, and electrolytes between various parts of the plant. Transport in both systems is pressure-driven, but while the pressure that drives xylem transport is extrinsic to the system—that is, the requisite energy comes from atmospheric evaporation from leaf surfaces—the pressure in the phloem is produced by osmotically induced gradients in free energy and depends on the loading and unloading of solutes at the "source" and "sink" ends of the translocation pathway. Hydrostatic pressure increases osmotically at the source as solutes, such as sucrose, oligosaccharides, sugar alcohols, electrolytes, amino acids and certain

*Corresponding author. Tel.: +1-617-496-3580; fax: +1-617-496-5854.
E-mail address: thompson@fas.harvard.edu (M. V. Thompson).

0022-5193/03/$35.00
© 2003 Elsevier Science Ltd. All rights reserved.

organic and inorganic acids (Ziegler, 1975; Zimmermann & Ziegler, 1975), are secreted into the phloem conduit, and decreases at the sink where those solutes are removed. The resulting hydrostatic pressure gradient drives these solutes from their "sources" to their "sinks", a type of transport system called "osmotically generated pressure flow" (OGPF). This mechanism was first described for the phloem in the early part of the 20th century (Münch, 1926, 1927, 1930) and is currently the primary candidate mechanism for long-distance metabolite transport in plants (Komor *et al.*, 1996; Köckenberger *et al.*, 1997; Ehlers *et al.*, 2000; Eckardt, 2001; Patrick *et al.*, 2001).

At present, confidence in the capacity of the OGPF hypothesis to account for observed rates of phloem translocation is sufficiently great that the resistance of the transport pathway itself is no longer considered limiting (Passioura & Ashford, 1974). Indeed, modeling (Tyree *et al.*, 1974; Goeschl & Magnuson, 1986) and empirical studies (Passioura & Ashford, 1974; Magnuson *et al.*, 1986) have shown the OGPF hypothesis—in its simplest form—to be a virtual certainty for small plants. Additionally, the relatively recent recognition that sieve plates are nominally clear of P-proteins further justifies this certainty (Knoblauch & van Bel, 1998; Eckardt, 2001; Knoblauch *et al.*, 2001), and has only bolstered the study of assimilate loading in source tissues (van Bel & Gamalei, 1992; van Bel, 1993; Komor *et al.*, 1996; Turgeon & Medville, 1998; Patrick *et al.*, 2001) and unloading in sink tissues (Oparka, 1990; Farrar, 1993; Minchin & Thorpe, 1996; Patrick, 1997; Oparka & Turgeon, 1999; Oparka & Cruz, 2000), as well as the molecular biology of the transfer of water, sucrose, and amine-nitrogen between the phloem and xylem (Patrick *et al.*, 2001).

When applied to long distances, however, the status of the OGPF hypothesis may be somewhat uncertain. While it is true that gradients in both pressure (Zimmermann & Brown, 1980) and solute potential (Hocking, 1980) have been found along the trunks of large plants, and transport velocities (of between 0.5 and $1.0\,m\,hr^{-1}$) have been measured that could cover the requisite distances over sufficiently short time-scales (Canny, 1973; Zimmermann & Brown, 1980), the presence of such gradients and transport rates does not necessarily satisfy as to mechanism. For instance, while Tyree *et al.* (1974) showed that OGPF is *feasible* over very long distances ($\sim 50\,m$), a quick calculation of the sap flux densities reported in their Fig. 7 shows that it would take over 15 days for sucrose to be transported over that distance, and even then only 1/50th of the sucrose would arrive in the final meter. This is unsatisfactory for a number of reasons. One would expect source tissues to be reasonably responsive to changes in assimilate consumption by sink tissues, but a transit time of 15 days would put the frequency response time of the source to no less than that order of magnitude. Moreover, molecules, such as hormones, which require short transit times for their functions to be meaningfully felt, would take so long to move from the leaves to the roots that their relevance to the plant would become somewhat dubious. Thus, as currently understood, the classical pressure-flow scheme of Münch may be insufficient over long distances. One way around this problem would be for the phloem to relay assimilates from one sieve tube to the next, thus making use of metabolic energy to overcome the high intrinsic and viscous resistances to flow (Lang, 1979; Aikman, 1980; Murphy & Aikman, 1989). This "relay hypothesis" leads to the suggestion that perhaps individual sieve tubes are quite short, though the transport distance is very long.

However, even over distances of a meter or less, there are a number of unanswered questions about how the plant controls the concentration of assimilates in the sieve tube, and how it is coordinated such that the assimilate concentration of a sieve tube does not alternately crash and boom with small deviations or phase shifts between loading and unloading. Many of these questions cannot be answered using the model systems currently in vogue. The shift in focus from long-distance transport—considered largely "solved" in the 1970s and 1980s—toward solute loading and unloading, both allowed and required that one work on plants whose transport pathways were relatively short. Until methodology

meets the task of directly experimenting with phloem transport in large plants and over long distances, our approach should include top-down analyses of the potential constraints on phloem transport, and the functioning of the phloem in the context of the entire vascular system. But to do so requires the construction of a model of non-steady-state phloem transport that can account for its mathematical nonlinearities, a model more sophisticated than any model currently available (Table 1).

Here, we present a fully implicit, finite-difference, 100% mass-balanced, sucrose-only solution to Münch pressure flow. The model can be solved for non-steady-state, temporally evolving aspects of the system, as well as for steady-state scenarios, and is composed of a pair of coupled, nonlinear partial differential equations, which require a numerical approach to be accurately solved. To our knowledge, only two non-steady-state models have been developed (Ferrier *et al.*, 1975; Smith *et al.*, 1980). In this paper, we communicate the numerical solution, present idealized results, test transport times over long distances, and test the sensitivity of the concentration of sucrose in the loading zone to variation in unloading rates. In the appendices, we present a complete description of the

TABLE 1

Summary and comparison of the characteristics of previous analytical and numerical models of Münch's osmotically generated pressure-flow hypothesis

	Non-steady-state?	Numerical or analytic?	Node boundary concentration?	Loading and unloading:	Nonlinear solute potential?	Elastic sieve tube?	Nonlinear viscosity?	Non-zero sucrose partial volume?	Sieve plates?	Axial flow:
This work	×	Numerical	SL-TVD	C	×	×	×	×	× +S	HP
Horwitz*		Analytic		C					×	HP
Eschrich and Young†		Analytic		A					×	HP
Tyree‡		Numerical	USN	C				×	×	HP
Ferrier and Christy§	×	Numerical	USN	CC			×	×	×	HP
Lang‖		Analytic		J			×		×	HP
Goeschl and Smith¶	×	Numerical	M	C				×	×	HP
Murphy**		Analytic		C			×	×	×	HP
Phillips††		Analytic		J				×		ST

* Horwitz (1958).
† Eschrich *et al.* (1972); Young *et al.* (1973).
‡ Tyree *et al.* (1974).
§ Christy & Ferrier (1973); Ferrier & Christy (1975); Ferrier *et al.* (1975); Ferrier (1978).
‖ Lang (1978).
¶ Goeschl *et al.* (1976); Smith *et al.* (1980).
** Murphy (1989b, 1989a).
†† Phillips & Dungan (1993).

Authors are cited by their entire body of work, and the features described are of their most advanced contributions. Key: ×—signifies presence; A—loading and unloading set to arbitrary, constant values, independent of concentration—mean tube concentration must also be set arbitrarily to obtain a unique solution; C—loading is set at a constant value while unloading is concentration dependent—provides unique solution; CC—both loading and unloading are concentration dependent—here, a unique solution is not obtained because it is not in a closed form (see Goeschl *et al.*, 1976; Magnuson *et al.*, 1979); HP—axial flow described by Hagen–Poiseuille flow equation; J—solute flux is set to a constant value throughout the tube, i.e., $\partial j_s/\partial z = 0$, and concentration at the upstream end is set to and held at some arbitrary value, i.e., $c(z = 0) = c_o$—here, a unique solution is always obtained; M—uses the equally weighted mean concentration of the adjacent nodes for the node boundary concentration; S—includes the Sampson factor for flow convergence around narrow pores—see Appendix B; SL-TVD—uses a slope-limiting total variation diminishing method for setting the concentration of the node boundary; ST—axial flow described by asymptotic analysis of Stokes equation; USN—uses the upstream node concentration for the node boundary concentration.

numerical methods used in this model, tests of model accuracy against spatial and temporal resolution, and justifications of the use of the Hagen–Poiseuille flow equation through sieve tubes and pores.

2. Model Description

Here we describe a robust, sucrose-only, non-steady-state, numerical solution to the OGPF hypothesis (Fig. 1), which makes a number of improvements to previous models, including wall elasticity, nonlinear functions of viscosity and solute potential, an enhanced calculation of sieve pore resistance, and the introduction of a slope-limiting total variation diminishing (TVD) method for determining the node boundary sucrose concentration (Table 1). A history of previous models of the OGPF hypothesis is given in Appendix A. Our formulation makes the following assumptions:

(1) The sieve tube walls are smooth with a circular perimeter, and are interspersed with transverse, perpendicular sieve plates that impose an additional resistance to bulk flow, adding in series to that of the sieve element lumen.

(2) The sieve plates are simple (that is, they contain only one sieve area) and the pores contained therein are all of equal size, circular shape, and equal length; they are distributed homogeneously throughout the plate, and have a zero-value reflection coefficient with respect to sucrose.

(3) The Hagen–Poiseuille flow relation governs the local axial movement of sap—laminar

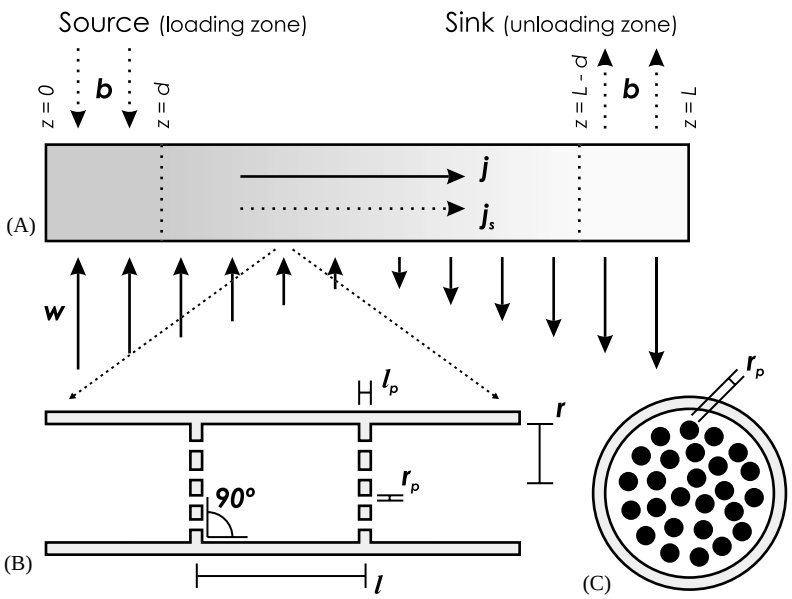

FIG. 1. A schematic of an idealized sieve tube. (A) Sucrose is loaded (b) at the "source" end of the sieve tube and unloaded at the "sink" end, leading to a gradient in sucrose concentration along the sieve tube (as shown by decreasing gray shading from source to sink). As sucrose concentration increases, water flows into the sieve tube (w) from the surrounding apoplast, following a gradient in water potential; as concentration decreases, water flows out. The pressure gradient generated by w (and by b, since the sucrose has a non-zero volume, thus affecting the pressure) is what induces the axial flow of both volume j and solute j_s. The sieve tube is of length L—where z denotes the distance along the tube from $z = 0$ to L—and is subdivided into three zones, the loading zone, the intermediate zone, and the unloading zone. The loading and unloading zones are both of length d, where the loading zone extends from $z = 0$ to d, and the unloading zone extends from $z = L-d$ to L. (B) The sieve tube is subdivided into cellular sections called sieve elements of length l and radius r. Each sieve element is bounded at its ends by a sieve plate of thickness l_p containing pores of radius r_p. Sieve plate resistance is several times greater than that of the sieve element lumen, i.e. $\beta \ll 1$, see Appendix B. (C) A longitudinal cross-section of a sieve element exposes the geometry of the sieve plate, which is shown here to be circular and possessing a regular array of equally sized, circular sieve plate pores. The model parameter α is the summed cross-sectional area of all the pores in the plate, divided by the transverse cross-sectional area of sieve element. Note that α can be greater than or equal to unity if the sieve plates are positioned obliquely instead of transversely as shown here.

flow with a parabolic velocity profile is rapidly established following entry to each sieve element, inertial and gravitational effects of the Navier–Stokes equation can be ignored, and despite a small amount of flow across the membrane walls, a parabolic velocity profile is maintained throughout the sieve element (Appendix B).

(4) Flow through the sieve pores is a linear function of the pressure difference across the sieve plate and is governed by the Hagen–Poiseuille flow relation plus an additional term called the Sampson factor, described in Appendix B.

(5) Sucrose is the only solute.

(6) The sieve tube plasma membrane is ideally semi-permeable, i.e. the reflection coefficient for sucrose is unity.

(7) Radial solute diffusion is rapid relative to axial convection such that the radial sucrose concentration gradient is effectively zero.

(8) Axial molecular diffusion and dispersion are small relative to axial solute convection, and can be ignored.

(9) The sieve tube's cross-sectional area expands with pressure in a linear elastic manner according to a generalized expression for the drained pore modulus (or volumetric elastic modulus) of the phloem tissue.

Assumptions (3) and (4) are justified in Appendix B while assumptions (7) and (8) are justified in Appendix C. Assumption (9) is justified if the volumetric expansion is small.

The initial and boundary conditions of the model are at the discretion of the user, provided that flow through the end walls of the tube (at $z = 0$ and L) is zero (Neumann boundary condition), where z (m) is the distance along the sieve tube and L (m) is the length of the sieve tube. All symbols are defined in the text and in Table 2. The governing equations are summarized in Table 3. Diagrams of the relevant control volumes are given in Fig. 2. Solutions are arrived at by numerically solving a coupled pair of nonlinear partial differential equations (PDEs) for the temporal and spatial evolution of pressure and sucrose in a long, linearly elastic, membrane element, where the membrane is semi-permeable to water, and sucrose is loaded into the membrane element at one end of the tube ($0 < z < d$) over a loading distance d (m) and unloaded at the other end of the tube ($L - d < z < L$) over the same distance d.

2.1. GOVERNING EQUATIONS

2.1.1. *Cross-Sectional Area*

The concentration of sucrose per unit length of sieve tube c_l [mol (m length)$^{-1}$] is equal to the concentration per unit volume c (mol m^{-3}) times the cross-sectional area of the tube a (m^2) :

$$c_l = ac, \tag{1}$$

and it is assumed that sucrose is homogeneously distributed with respect to r. The cross-sectional area of the sieve tube is assumed to be an elastic function of lumen pressure. If the length of the sieve tube is constant with pressure, then the drained pore modulus (or volumetric elastic modulus, in plant physiological terms) is given by $\varepsilon = V(\mathrm{d}p/\mathrm{d}V) = a(\mathrm{d}p/\mathrm{d}a)$, where

$$\frac{\mathrm{d}a}{\mathrm{d}p} = \frac{a}{\varepsilon}, \tag{2}$$

Here p (MPa) is the hydrostatic pressure in the sieve tube lumen, and ε (MPa) is the drained pore modulus of the phloem tissue. It is assumed, over a reasonable range of sieve tube pressures, that the drained pore modulus is constant, even though at modest strains this may not be the case (Wu *et al.*, 1985). Sieve tube cross-sectional area as a function of pressure is given by

$$\frac{a}{a_o} = \mathrm{e}^{(p-p_o)/\varepsilon}, \tag{3}$$

where a_o and p_o are the initial cross-sectional area and pressure of the sieve tube.

2.1.2. *Axial Flow*

The axial flux of sucrose j_s (mol s^{-1}) is the product of c and the axial flux of sap j (m^3 s^{-1}) :

$$j_s = cj. \tag{4}$$

TABLE 2
Summary of symbols

Symbol	Description	Units
a, A_i	Cross-sectional area of sieve tube	m^2
a_s	Activity of sucrose	mol (kg solution)$^{-1}$
b, B_i	Sucrose loading (or unloading) rate	mol (m length)$^{-1}$ s^{-1}
b_{unload}	Mean unloading rate in the unloading zone	mol (m length)$^{-1}$ s^{-1}
c, C_i	Sucrose concentration	mol m^{-3}
δC_i^m	Concentration correction term	mol m^{-3}
c_l	Length-specific sucrose concentration	mol (m length)$^{-1}$
c_{load}	Mean concentration in the loading zone	mol m^{-3}
c_{unload}	Mean concentration in the unloading zone	mol m^{-3}
Cr	Courant number, $Cr = v\Delta t/\Delta z$	Dimensionless
c^*	Set point sucrose concentration for unloading zone	mol m^{-3}
d	Length of loading or unloading zone	m
D_i	Coefficient of membrane water flux defined in eqn (D.10)	m^3 (m length)$^{-1}$ s^{-1} MPa^{-1}
D_m	Molecular diffusion coefficient	m^2 s^{-1}
f	Spatial node frequency (N/L)	nodes (m length)$^{-1}$
F_i	Bookkeeping coefficient defined in eqn (D.34)	mol (m length)$^{-1}$(m^2 cross-section)$^{-1}$ MPa^{-1}
G_i	Derivative of ψ_π with respect to c	MPa (mol m^{-3})$^{-1}$
H_i	Bookkeeping coefficient defined in eqn (D.21)	m^3 (m length)$^{-1}$ s^{-1} MPa^{-1}
i	Subscript referring to node number (e.g.: $A_i^{n+1,m}$, which is a in node i at time step number $n+1$ and iteration number m)	Dimensionless
j, J_i	Axial volume flux rate in sieve tube	m^3 s^{-1}
δJ_i^m	Axial volume flux rate correction term	m^3 s^{-1}
j_s, $J_{s,i}$	Axial molar flux rate of sucrose in sieve tube	mol s^{-1}
j_p	Volume flux rate through a single sieve pore	m^3 s^{-1}
k	Axial conductivity of sieve tube defined in eqn (6)	m^3 (m length) s^{-1} MPa^{-1}
K	Axial conductance of sieve tube defined in eqn (D.19)	m^3 s^{-1} MPa^{-1}
l	Distance between sieve plates (the length of a sieve element)	m
l_p	Thickness of sieve plate	m
L	Length of the sieve tube (the transport distance)	m
L_p	Sieve tube plasma membrane permeability	m^3 (m^2 membrane area)$^{-1}$ s^{-1} MPa^{-1}
m	Superscript referring to the iteration number (see i), also the molality of a sucrose solution (same units as a_s)	Dimensionless
n	Superscript referring to the time step number (see i)	Dimensionless
N	Number of nodes in the model domain	Dimensionless
N_p	Number of sieve pores per sieve plate	Dimensionless
p, P_i	Hydrostatic pressure in sieve tube lumen	MPa
δP_i^m	Pressure correction term	MPa
Δp_{lumen}	Axial pressure drop within a single sieve element (not including sieve plates)	MPa
Δp_{pore}	Pressure drop across a single sieve pore due to the Hagen–Poiseuille (H–P) pressure drop alone	MPa
Δp^*_{pore}	Total pressure drop across a single sieve pore, including both the H–P and Sampson (S) pressure drops	MPa
$\Delta p_{pore,Sampson}$	Pressure drop across a single sieve pore due to the S effect alone	MPa
Δp_T	Total axial pressure drop over a single sieve element plus an adjoining sieve plate	MPa
Q_i	Estimate of δC^m used in solution of eqn (D.28)	mol m^{-3}
r, R_i	Radius of sieve tube	m
r_p	Radius of sieve pores	m
$\Re$	Universal gas constant	MPa m^3 kg^{-1} K^{-1}
S_i	Bookkeeping coefficient defined in eqn (D.16)	m^3 (m length)$^{-1}$ s^{-1}
t	Time	s; hr
Δt	Time step length	s
T	Temperature	K

TABLE 2 (*continued*)

Symbol	Description	Units
U_i	Bookkeeping coefficient defined in eqn (D.34)	mol (m^2 cross-section)$^{-1}$ (m length)$^{-1}$
v	Sap flux density	m s^{-1}; cm hr^{-1}
v_s	Axial molar flux density of sucrose ($d<z<L-d$)	mol (m^2 cross-section)$^{-1}$ s^{-1}
v_s'	v_s at steady state in the intermediate zone ($d<z<L-d$)	mol (m^2 cross-section)$^{-1}$ s^{-1}
V_i	Volume of sieve tube	m^3
$\overline{V_s}$	Partial molal volume of sucrose	m^3 mol^{-1}
w, W_i	Membrane water flux rate	m^3 (m length)$^{-1}$ s^{-1}
X_i	Generic state variable	Dimensionless
δX_i^m	Generic state variable correction term	Dimensionless
z	Axial distance along the sieve tube	m
Δz	Node length	m
α	Ratio of combined cross-sectional area of the sieve pores to the transverse cross-sectional area of sieve tube	Dimensionless
β	Sieve plate impedance factor	Dimensionless
γ_s	Activity coefficient of sucrose	Dimensionless
ε	Phloem tissue drained pore modulus	MPa
ζ	Relative amplitude of sine impulse function	Dimensionless
η_z	Energy dissipation in axial flow of sieve tube sap	J m^{-1} s^{-1}
η_c	Energy dissipation in loss of sucrose chemical potential	J m^{-1} s^{-1}
η_r	Energy dissipation in flow of water across bounding membranes	J m^{-1} s^{-1}
θ	System state; pressure–volume or concentration–volume	MJ; mol
μ	Dynamic viscosity of sieve tube sap	MPa s
μ_s	Chemical potential of sucrose	MJ mol^{-1}
μ_s^*	Chemical potential of sucrose at standard state	MJ mol^{-1}
ρ_w	Density of water	kg m^{-3}
σ	The standard deviation	Dimensionless
τ	Transit time	s; hr
ϕ	Phase shift	s; hr
φ	Sampson factor	Dimensionless
χ	Fractional displacement of the current system state from steady state (convergence estimate)	Dimensionless
ψ^o, Ψ_i^o	Water potential of the apoplast external to the sieve tube	MPa
ψ_π, $\Psi_{\pi,i}$	Solute potential of sieve tube sap	MPa
$\delta\Psi_{\pi,i}^m$	Solute potential correction term	MPa

When paired, the upper case letter refers to the discrete version of the lower case letter.

Note that we neglect an axial diffusion term (see Appendix C). Axial sap flow is calculated locally according to the Hagen–Poiseuille flow relation (see Appendix B):

$$j = -k\frac{\partial p}{\partial z}, \tag{5}$$

where k [m^3 (m length) s^{-1} MPa^{-1}] is the hydraulic conductivity of the sieve tube (assuming cylindrical geometry):

$$k = \beta\frac{\pi r^4}{8\mu}. \tag{6}$$

Here μ (MPa s) is the dynamic viscosity of the solution as a function of sucrose concentration and temperature (Bouchard & Grandjean, 1995), and r (m) is the sieve tube radius. Temperature is set to a constant 293 K throughout the model domain. The dimensionless sieve plate factor β (derived in Appendix B) is given by

$$\beta = \frac{\alpha\varphi r_p^2 l}{\alpha\varphi r_p^2(l-l_p) + r^2 l_p}, \tag{7}$$

and represents the degree to which the presence of sieve plates reduces the conductivity of the

TABLE 3

Summary of state variables and governing equations used in this simulation, as well as the fully expanded analytical equations for volume and sucrose conservation

Description	Governing equations	Boundary and initial conditions
State variables and initial conditions	$p = p(z,t)$ $c = c(z,t)$ $r = r(z,t)$ } for $0 < z < L$	$p(z,0) = 0$ $c(z,0) = 0$ $r(z,0) = r_o(z)$ $a_o(z) = \pi r_o(z)^2$
Cross-sectional area and concentration	$c_l = a\,c$	
Cross-sectional area and pressure	$\frac{da}{dp} = \frac{a}{\varepsilon}$	$\frac{a}{a_o} = e^{(p-p_o)/\varepsilon}$
Axial flow of sucrose	$j_s = c\,j$ (with slope limits)	
Axial flux of solution	$j = -k\frac{\partial p}{\partial z}$	$j = 0$ for $z = 0, L$
Passive membrane water flux (ψ_π = nonlinear function of c)	$w = 2\pi r L_p[\psi^o - (p + \psi_\pi)]$	$\psi^o(z,t) = 0$
Volume conservation statement	$\frac{\partial a}{\partial t} = \overline{V_s} b + w - \frac{\partial j}{\partial z}$	
Solute conservation statement	$\frac{\partial c_l}{\partial t} = b - \frac{\partial j_s}{\partial z}$	
Loading and unloading of sucrose		$b = \frac{a v_s'}{d}$, $0 < z < d$ $b = 0$, $d < z < L - d$, $b = -\frac{a v_s' c}{d\ c^*}$, $L - d < z < L$

Note: Fully expanded volume conservation equation

$$\frac{a(p)}{\varepsilon}\frac{\partial p}{\partial t} = \overline{V_s} b(c,t,z) + 2\pi r(p) L_p[\psi^o(t,z) - (p + \psi_\pi(c,T))] + \frac{\partial}{\partial z}\left[\beta \frac{\pi r(p)^4}{8\mu(c,T)}\frac{\partial p}{\partial z}\right].$$

Fully expanded sucrose conservation equation

$$\frac{ca(p)}{\varepsilon}\frac{\partial p}{\partial t} + a(p)\frac{\partial c}{\partial t} = b(c,t,z) + \frac{\partial}{\partial z}\left(c\beta \frac{\pi r(p)^4}{8\mu(c,T)}\frac{\partial p}{\partial z}\right).$$

The solution of these equations finds p and c as a function of distance along the sieve tube z and as a function of time t.

sieve tube. α is the combined cross-sectional area of all pores in the plate divided by the transverse cross-sectional area of the sieve tube (dimensionless), r_p (m) is sieve pore radius, l (m) is sieve element length or the distance between sieve plates, l_p (m) is pore length, and φ is the

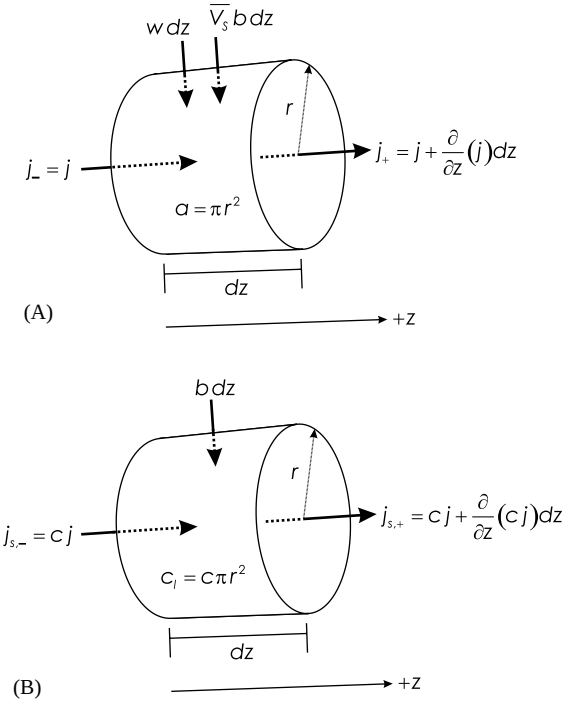

FIG. 2. (A) A diagrammatic outline of the volume conservation control volume used in this simulation. Fluxes included in volume conservation are the axial fluxes, across both the z- and $z+$ faces, the membrane water flux w, the sucrose loading flux b, and the volumetric expansion of the sieve tube. (B) A diagrammatic outline of the sucrose conservation control volume. Included are the axial fluxes, the sucrose loading flux, and the change in solute content of the control volume. See Section 2.1.4 for more details.

dimensionless Sampson factor, incorporating the non-zero resistance of zero-length sieve pores (see Appendix B).

2.1.3. *Membrane Water and Sucrose Flux*

The irreversible flow of water w [m^3 (m length)$^{-1}$ s^{-1}] across the plasma membrane is positive inward (Kedem & Katchalsky, 1958):

$$w = 2\pi r L_p[\psi^o - (p + \psi_\pi)], \tag{8}$$

where L_p [m^3 (m^2 membrane area)$^{-1}$ s^{-1} MPa^{-1}] is the membrane permeability, ψ^o (MPa) is the water potential of the surrounding apoplast, and ψ_π (MPa) is the phloem sap's osmotic potential (or solute potential, as it has been historically referred to in the plant physiology literature), given by (Michel, 1972) :

$$\psi_\pi = -\rho_w \Re T(0.998\ m + 0.089\ m^2), \tag{9}$$

where ρ_w [998.03 kg m^{-3}] is the density of water, $\Re$ (8.3143×10^{-6} MPa m^3 kg^{-1} K^{-1}) is the universal gas constant, and T (K) is the temperature of the solution. m is the molality [mol (kg of solvent)$^{-1}$]:

$$m = \frac{c}{\rho_w(1 - c\overline{V_s})}, \tag{10}$$

where $\overline{V_s}$ [2.155×10^{-4} m^3 mol^{-1}] is the partial molal volume of sucrose (Eszterle, 1993), which is independent of concentration as long as the solution is sub-saturated.

Sucrose loading and unloading into and out of the sieve tube b [mol (m length)$^{-1}$ s^{-1}] is one of the boundary conditions of the simulation defined by the user and is defined on a unit length basis. The product of b and $\overline{V_s}$ is the volume flux of sucrose into and out of the sieve tube.

2.1.4. *Conservation Equations*

Mass conservation of solution and sucrose are described by PDEs based on an appropriate pair of control volumes, one for volume and the other for sucrose conservation (Fig. 2). Volume conservation is given by the following continuity equation:

$$\frac{\partial a}{\partial t} = \overline{V_s}b + w - \frac{\partial j}{\partial z}. \tag{11}$$

We recognize that volume is not typically considered a conserved quantity, but it is analytically more straightforward than mass, and in this system, where ρ_w and $\overline{V_s}$ are held constant, the substitution of volume for mass is allowed.

The conservation of sucrose is written as

$$\frac{\partial c_l}{\partial t} = b - \frac{\partial j_s}{\partial z}, \tag{12}$$

which, after inserting eqns (1) and (4), gives

$$\frac{\partial (ca)}{\partial t} = b - \frac{\partial (cj)}{\partial z}. \tag{13}$$

2.1.5. *Coupled System of PDEs*

Equations (11) and (13) are a system of coupled, nonlinear PDEs, and can be expressed entirely in terms of pressure and concentration, where T, ψ^o, and b are prescribed:

$$\frac{a(p)}{\varepsilon}\frac{\partial p}{\partial t} = \overline{V_s} b(c,t,z) + 2\pi r(p) L_p [\psi^o(t,z) - (p + \psi_\pi(c,T))] + \frac{\partial}{\partial z}\left[\beta \frac{\pi r(p)^4}{8\mu(c,T)}\frac{\partial p}{\partial z}\right], \quad (14)$$

where ψ^o is a function of time and distance along the sieve tube, b is a function of concentration, distance and time, ε, $\overline{V_s}$, L_p and β are constant model parameters, a and r are functions of pressure according to eqn (3), and ψ_π and μ are functions of concentration and temperature. The sucrose conservation equation can be similarly expanded:

$$\frac{ca(p)}{\varepsilon}\frac{\partial p}{\partial t} + a(p)\frac{\partial c}{\partial t} = b(c,t,z) + \frac{\partial}{\partial z}\left(c\beta \frac{\pi r(p)^4}{8\mu(c,T)}\frac{\partial p}{\partial z}\right). \quad (15)$$

Note that coupled systems of nonlinear PDEs of this kind cannot be solved analytically, and that the analytical expansion of eqns (11) and (13) given in eqns (14) and (15) cannot be discretized given the inapplicability of the chain rule over large changes in p or c at low spatial or temporal resolutions. Instead, our approach, as outlined in the following section and Appendix D, is to prepare eqns (11) and (13) for numerical analysis by spatial and temporal discretization. Equations (14) and (15) can be viewed as guides to the complexities and nonlinearities of modeling solute transport in a narrow semi-permeable membrane-bound system. Note that we have not explicitly included gravitational effects because they are only important in the presence of large differences in the density of xylem and phloem sap, as discussed in Appendix B (see also Milburn, 1975).

2.2. DISCRETIZATION OF GOVERNING EQUATIONS

We use a fully implicit, finite-difference approach to the solution of eqns (11) and (13) described in Appendix D (Nielsen *et al.*, 1986; Milly, 1988; Istok, 1989; Celia *et al.*, 1990), known as the modified Newton–Raphson method, with a slope-limiting TVD method for determining sucrose concentrations at node boundaries in regions with sharp and fast-moving concentration fronts (Ewing & Wang, 2001). The use of these methods dramatically improves the stability and accuracy of the solution over other time-discretization methods. To denote time step and iteration number, we use the notation of Celia *et al.* (1990), where the superscript n denotes time step number and the superscript m denotes iteration number (Appendix D). For a clear explication of the numerical methods implemented here, the groundwater and unsaturated soil water flow literature is particularly useful (Wang & Anderson, 1982; Nielsen *et al.*, 1986; Milly, 1988; Istok, 1989; Celia *et al.*, 1990).

Equations (11) and (13) are rewritten in their discrete form:

$$\frac{\partial}{\partial t}(A_i^{n+1,\,m+1}) = W_i^{n+1,\,m+1} + \overline{V_s} B_i^{n+1,\,m} - \frac{\partial}{\partial z}(J_i^{n+1,\,m+1}), \quad (16)$$

and

$$\frac{\partial}{\partial t}(C_i^{n+1,\,m+1} A_i^{n+1,\,m+1}) = B_i^{n+1,\,m} - \frac{\partial}{\partial z}(C_i^{n+1,\,m+1} J_i^{n+1,\,m+1}). \quad (17)$$

The simulated sieve tube is subdivided into nodes of length Δz denoted by the subscript i, into time steps of length Δt denoted by the superscript n, and into iterations within those time steps denoted by m. Because B is prescribed, it is written in terms of the $(n+1, m)$-th iteration in contrast to the other variables. Note in eqns (16) and (17) that A depends on pressure, B on concentration, and W and J on pressure (including gradients in pressure) and concentration. The use of the

$(n+1)$st time step is indicative of the backward-differencing or fully implicit method employed (Appendix D). In each iteration, eqn (16) is solved for a pressure correction term (according to the modified Newton–Raphson method), from which revised pressures, axial flow rates and cross-sectional areas are calculated. The revised estimates of J and A are then used to solve eqn (17) for the sucrose concentration correction term. Sucrose concentrations are then revised, and the state of the system is checked for mass conservation. If volumetric and solute conservation is not met, another iteration is performed, using the new estimates of P and C as baselines for the next set of corrections, as well as the basis for recalculating K (conductance) and B (loading rate). The test for conservation of volume and solute is discussed in Appendix E.

2.3. SUCROSE LOADING AND UNLOADING AND GRADIENTS IN EXTERNAL WATER POTENTIAL

Sucrose loading and unloading can be defined in terms of t and z in any number of ways, as long as there is a closed-form solution (Goeschl *et al.*, 1976). In this work, sucrose is loaded and unloaded in the loading and unloading zones such that in the intermediate zone, at steady state, the axial sucrose flux density v_s' is $0.225\,\mathrm{mol\,(m^2\,cross\text{-}section)^{-1}\,s^{-1}}$ (Lang, 1978). With this condition, b is given by

$$\left.\begin{array}{rl} b = \dfrac{av_s'}{d}, & 0<z<d, \\ b = 0, & d<z<L-d, \\ b = -\dfrac{av_s'}{d}\dfrac{c}{c^*}, & L-d<z<L, \end{array}\right\}, \qquad (18)$$

where c^* is a concentration set point (set arbitrarily to $500\,\mathrm{mol\,m^{-3}}$). c^* imposes a concentration boundary condition on the unloading zone, where at steady state the mean concentration in that zone, c_{unload}, equals c^*. Conversely, the mean concentration in the loading zone, c_{load}, is set by v_s'. Here, $d = 0.5\,\mathrm{m}$ and $r = 7.5\times10^{-6}\,\mathrm{m}$, so in the loading zone b is $7.952\times10^{-11}\,\mathrm{mol\ (m\ length)^{-1}\,s^{-1}}$.

The water potential of the surrounding phloem tissue ψ^o is also prescribed by the user. Here, to simplify, it is set to 0.0 MPa for all t and z.

2.4. ENERGY DISSIPATION AS AN INDEX OF RESISTANCE

The movement of solution through the sieve tube system is primarily limited by two passively resistive factors, the resistance to axial flow through the sieve elements and across the sieve plates, and the resistance to water transport across the plasma membrane. To compare the relative contributions of membrane vs. axial flux in resisting the flow of sap through the sieve tube, we use the irreversible energy dissipation rate of the two processes as a proxy.

According to irreversible thermodynamics, dissipative energy loss is the product of the flow rate and the gradient in potential energy driving that flow. Because the application of the Hagen–Poiseuille flow relation is locally justified, this approximation is very good. For axial sap flow, energy dissipation η_z [J (m length)$^{-1}$ s^{-1}] is given by

$$\eta_z \approx -j\frac{\mathrm{d}p}{\mathrm{d}z}\times10^6. \qquad (19)$$

The factor 10^6 is the conversion from MJ to J, which is a more convenient unit. Flow across the bounding membrane dissipates energy at a rate η_r [J (m length)$^{-1}$ s^{-1}], where

$$\eta_r \approx w(\psi^o - p - \psi_\pi)\times10^6. \qquad (20)$$

Energy stored in the chemical potential of the sucrose is also lost as a drop in pressure and concentration, lowering the useful work the sucrose can perform as it is unloaded. This dissipation η_c [J (m length)$^{-1}$ s^{-1}] is given by

$$\eta_c \approx -j_s\frac{\mathrm{d}\mu_s}{\mathrm{d}z}\times10^6, \qquad (21)$$

where μ_s (MJ mol^{-1}) is the chemical potential of sucrose in solution, given by

$$\mu_s = \Re T\ln a_s + \overline{V_s}p + \mu_s^*, \qquad (22)$$

where μ_s^* (MJ mol^{-1}) is the chemical potential of sucrose at standard state (this drops out since it is a constant within the model domain), and a_s [mol (kg of solution)$^{-1}$] is the activity of sucrose

in solution given by

$$a_s = \gamma_s m, \tag{23}$$

where γ_s (dimensionless) is the activity coefficient. We assume that γ_s does not change with concentration, so it also drops out. The gradient in chemical potential from one point in the sieve tube (a) to the next (b), assuming the activity coefficient of sucrose varies little between those points, is given, following integration, by

$$\left.\frac{\Delta\mu_s}{\Delta z}\right|_{a\to b} = \frac{(\Re T \ln m_b + \overline{V_s} p_b) - (\Re T \ln m_a + \overline{V_s} p_a)}{\Delta z}. \tag{24}$$

Integrating each of these quantities, η_z, η_r, and η_c, across the model domain gives the total energy consumption of each irreversible flux.

3. Results and Discussion

The phloem model constructed in this work, implemented in MATLAB v6.1 (The MathWorks, Inc., Natick, MA, U.S.A.) and available from the authors upon request (Phloem Simulation, v2.2, Harvard University), is robust, even under sharp, fast-moving concentration fronts, and provides stable results to Courant numbers of upto $Cr = 0.4$ (see Appendix F). The following section describes example output from the simulation, calculates the dissipative energetic losses due to frictional and chemical potential dilution effects, and explores the steady-state and non-steady-state implications of the OGPF hypothesis over long distances.

All simulations in this paper describe a sieve tube of length $L = 5\,\text{m}$, and loading and unloading zone of lengths $d = 0.5\,\text{m}$ at opposite ends of the tube (see Fig. 1 for geometry), unless otherwise noted. The steady-state sucrose flux density v_s' in the intermediate zone is $0.225\,\text{mol}\,(\text{m}^2\ \text{cross-section})^{-1}\,\text{s}^{-1}$, with a concentration set point c^* of $500\,\text{mol}\,\text{m}^{-3}$, as described in Section 3.3. The tissue drained pore modulus ε is 17 MPa (Lee, 1981; Sovonick-Dunford *et al.*, 1982), and the membrane conductivity L_p is set to $5.0 \times 10^{-8}\,\text{m}^3\,(\text{m}^2\ \text{membrane area})^{-1}\,\text{s}^{-1}\,\text{MPa}^{-1}$ (Tyree, 1970; Lang, 1978). The external tissue water potential ψ^o is set to 0.0 MPa.

We use the sieve plate geometry of Lang (1978). Each sieve element has an initial radius r of 7.5 μm and has a fixed length l of 250 μm. The sieve plate thickness l_p is 0.5 μm, with a sieve pore radius r_p of 0.23 μm, the combined areas of which comprise 50% ($\alpha = 0.5$) of the total cross-sectional area of the sieve tube (in this case, approximately 530 sieve pores per plate). These values are consistent with those given by Weatherley & Johnson (1968) and summarized by Tyree *et al.* (1974). Following eqn (7), this geometry imposes an axial flow reduction factor β of 0.132, i.e. axial conductivity under this geometry is 13.2% of its value in the absence of sieve plates.

3.1. Example of non-steady-state results: a sharp concentration front

To demonstrate the numerical stability of the simulation, it is necessary to expose it to an extreme situation, in this case the approach to steady state from a zero-pressure, zero-concentration initial condition. In nature, concentration fronts this large or abrupt would be seldom found, nor is it likely that such a large jump in loading rate (in this case from zero) would ever be observed. However, trust in the model can be effectively established if exposed to extreme conditions. The results of a 1-day simulation of the time evolution of pressure, sucrose concentration, axial solution flux, and membrane water flux are shown in Fig. 3, and the results at 24 hr are qualitatively similar to the steady-state results of other workers (Christy & Ferrier, 1973; Tyree *et al.*, 1974; Goeschl *et al.*, 1976). Here the spatial resolution is $f = 200\,\text{nodes}\,\text{m}^{-1}$, and the time step length is $\Delta t = 1.0\,\text{s}$. The influx of water progressively dilutes the sucrose, leading to a drop in c and an increase in j with z (Tyree *et al.*, 1974; Phillips & Dungan, 1993). The pressure front propagates ahead of the sucrose front, creating a zone beyond the sucrose front where water is osmotically driven from the sieve tube, and just behind it where water is osmotically drawn from the surrounding tissue.

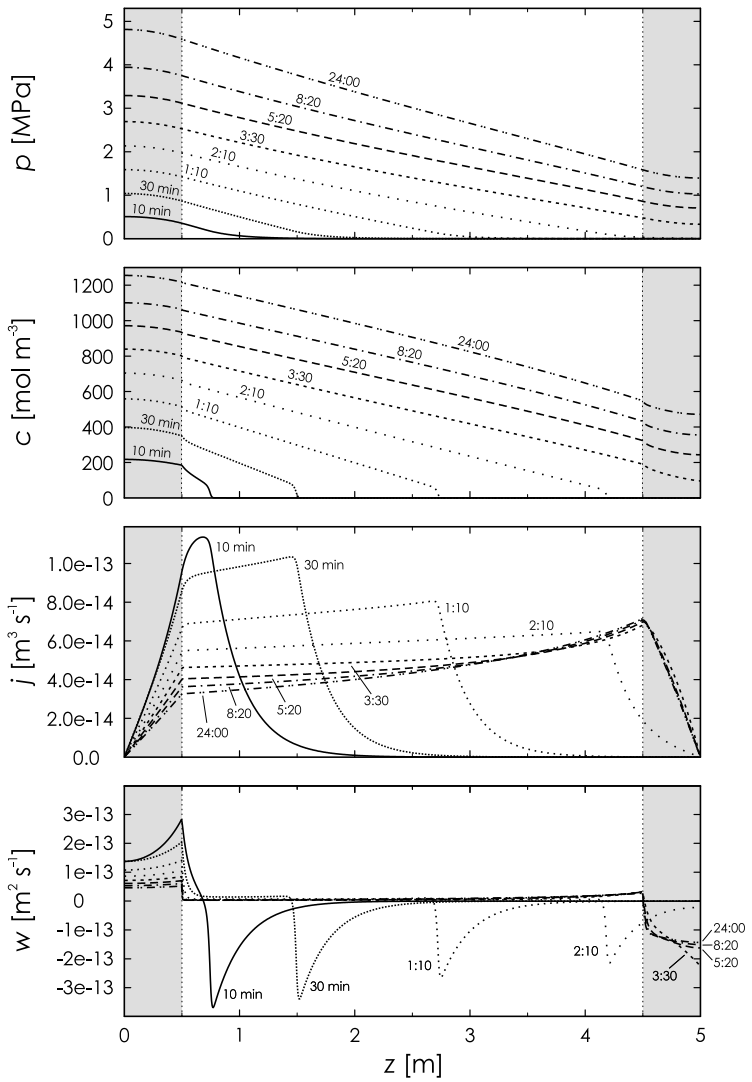

FIG. 3. The time evolution over a 24 hr period of pressure p, concentration c, axial volume flux j, and membrane water flux w in an idealized sieve tube of length $L = 5$ m, and high spatial ($f = 200$ nodes m^{-1}) and temporal ($\Delta t = 1$ s) resolution, as described in Section 3.1. The simulation is begun with the initial conditions $r(z,0) = 7.5 \times 10^{-6}$ m, $p(z,0) = 0$ MPa, and $c(z,0) = 0$ mol m^{-3}, and is performed with an axial sucrose flux density v_s' of 0.225 mol (m^{2}of cross-section)$^{-1}$ s^{-1}, corresponding to a constant loading zone sucrose membrane flux b of 7.952×10^{-11} mol (m length)$^{-1}$ s^{-1}. As in all simulations described in this paper, ε is set to 17.0 MPa, c^* to 500 mol m^{-3}, L_p to 5.0×10^{-8} m^3 (m^2 of membrane area)$^{-1}$ s^{-1} MPa^{-1}, ψ^o to 0.0 MPa, l to 250 μm, l_p to 0.5 μm, r_p to 0.23 μm, and α to 0.5. From the sieve plate geometry employed here, we calculate a β value of 0.132—i.e. sieve tube axial conductivity is only 13% of what it would be in the absence of sieve plates. The gray-shaded areas represent the loading (left) and unloading (right) zones of the model domain, each of length $d = 0.5$ m.

Sap flux density v (velocity) is at its greatest at this point.

The sucrose front develops in the first 0.5 m of the tube and requires 3.0 hr to reach the far end. The simulation comes to within 5% of steady state for both pressure and sucrose concentration after approximately 17 hr, and by the end of the simulation, at 24 hr, sucrose content has come to approximately 1.3% of steady state, while pressure-volume has come to within 1.7%. The derivation of these convergence estimates is given in Appendix E.

Sovonick-Dunford *et al.* (1982) measured the drained pore modulus of phloem tissue and, assuming the sieve tubes expanded with the same elastic coefficient as the bulk tissue, inferred a

sieve tube modulus of 17 MPa, conjecturing that this expansibility could increase the conductivity in periods of transiently high pressure (Lee, 1981; Sovonick-Dunford *et al*., 1982). It appears, however, that in the presence of sieve plates, an expansion-driven increase in conductivity would be relatively modest. We found that the pressurization, from 0.0 MPa at $t = 0$ hr to a mean pressure of 3.05 MPa at $t = 24$ hr, led to a sieve tube expansion of 20% from an initial volume of $0.88\,\text{mm}^3$, which corresponded to a 9.4% increase in radius. In the absence of sieve plates, this increase in radius would mean a 43.5% increase in axial conductivity, but in the presence of sieve plates there is almost no increase at all.

The mean concentration of sucrose in the sieve tube at steady state is $892\,\text{mol}\,\text{m}^{-3}$ (27.5% w/w), corresponding to a solute potential of -3.05 MPa, equal and opposite in magnitude to the hydrostatic pressure. The pressure gradient along the entire sieve tube is $-0.68\,\text{MPa}\,\text{m}^{-1}$, and $-0.75\,\text{MPa}\,\text{m}^{-1}$ excluding the loading and unloading zones. The mean steady-state sap velocity is $v = 2.0 \times 10^{-4}\,\text{m}\,\text{s}^{-1}$ (or $73.2\,\text{cm}\,\text{hr}^{-1}$).

We calculated the dissipative loss of energy associated with axial and membrane fluxes, and the drop in the chemical potential of sucrose as it flows along the sieve tube, η_z, η_r, and η_c, respectively (Fig. 4). Over the entire model domain, these losses account for dissipative energy fluxes of 1.51×10^{-7}, 3.98×10^{-9}, and $7.36 \times 10^{-9}\,\text{J}\,\text{s}^{-1}$, respectively. Irreversible energy dissipation in axial flow is over 40 times greater than loss due to wall flow, and it would be fair to assume that transport under this geometry and these boundary conditions is limited predominantly by axial resistance to flow, and that resistance to the membrane transport of water plays only a minor role.

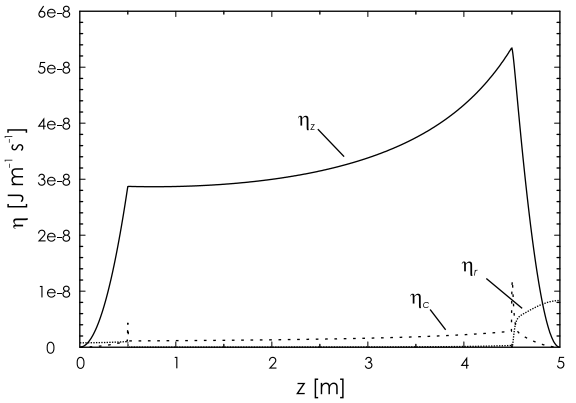

FIG. 4. Energy dissipation as a function of distance along the sieve tube due to the axial bulk flow of solution η_z, the flow of water across the bounding membrane η_r, or the loss in chemical potential of sucrose with distance along the tube η_c. Energy dissipation in this system is dominated by the axial resistance of the sieve tube and sieve plates. This suggests that the majority of the "resistance" to phloem transport is due to the sieve plates (i.e., $\beta = 0.132$), and that the conductivity of the membranes bounding the sieve element lumina is more than enough at this surface-to-volume ratio to accommodate membrane water transport. The decline in chemical potential during transport does not appear to be a significant dissipative loss.

3.2. LONG-DISTANCE TRANSPORT

The purpose of producing such a detailed and robust model of non-steady-state OGPF is to answer questions about the limitations of the theory over very long distances, and to determine the sensitivity of sieve tube concentration to changes in loading and unloading rate. With a steady-state model, only the first-order transport characteristics of the system can be calculated—such as the time it takes for solute to go from one end to the other, or the transport velocity or resistance. However, in cases where loading or unloading rates changes in a non-uniform manner, or both the apoplastic water potential and loading rates are varied simultaneously, a steady-state model would obviously be insufficient. In this section, we present steady-state results for *ceteris paribus* sieve tubes of varying lengths to calculate the limiting effect that increasing distance could have on the proper physiological functioning of the plant. We are not attempting to determine absolute efficacy, answering questions like "does long-distance transport work at distances over 25 m?", as it would be impossible to do so except on a species by species basis using studies of anatomy and physiology far more detailed than those available to us here. Rather, we wish to know the effect of increasing the sieve tube's length on its function. After presenting steady-state results, we give non-steady-state results that show the effect of small diurnal perturbations in unloading rate on the concentration of sucrose in the loading and unloading zones.

3.2.1. *Transport Distance*

Five simulations were performed to within 0.001% of steady state for sieve tubes matching the geometry of the sieve tube described in Section 3.1, but with different lengths $L = 1$, 2, 5, 10, and 20 m. We imposed the arbitrary boundary condition that the mean loading zone concentration c_{load} be equal to 1250 mol m^{-3} (37% w/w sucrose) and that the mean unloading zone concentration c_{unload} be equal to 500 mol m^{-3} (16.1% w/w sucrose). c_{unload} is set automatically during the course of a simulation by eqn (18) to equal c^*, but c_{load} can only be set by varying the loading rate b. As such, each sieve tube simulation was performed iteratively until we found the value of b that gave us a value of c_{load} equal to 1250 mol m^{-3}. c_{load} was set arbitrarily high to give liberal estimates of sap flux density, and for the sake of argument make as good a case as possible for transport over very long distances.

Figure 5 shows diagnostic data for each of these five simulations, including the sap flux density v (m s^{-1}), the solute flux density v_s [mol (m^2 cross-section)$^{-1}$ s^{-1}], the transit time τ (hr) through the sieve tube, and the ratio of axial to radial irreversible energy dissipation (which we hold as a proxy for the resistance of the axial path relative to the resistance of membrane walls). Sap flux density drops nearly two orders of magnitude between the 1-m and the 20-m sieve tube, and solute flux density does the same. We would expect the drop in both of these flux densities to be inversely proportional to the increase in sieve tube length, and this is indeed what we find, with some small deviations for shorter tubes due to the relatively high impact of membrane resistance to the total resistance of the sieve tube at shorter lengths. The sap flux density we calculate for the 1-m case is very high, 50% higher than even the fastest transport rates observed in the roots of *Triticum aestivum* by Passioura & Ashford (1974), and over a distance three times as long. This is largely due to the large concentration difference we applied.

Transit times τ increase by over three orders of magnitude with an increase in sieve tube length, from just 7 min at 1 m, to 7 hr at 5 m, to nearly 5 days at 20 m. This increase in τ is proportional to the square of the sieve tube length, which is sensible given that v decreases inversely with L. That a 20 m tube would require such a long transit time, even for a large concentration difference, begs the question of whether long

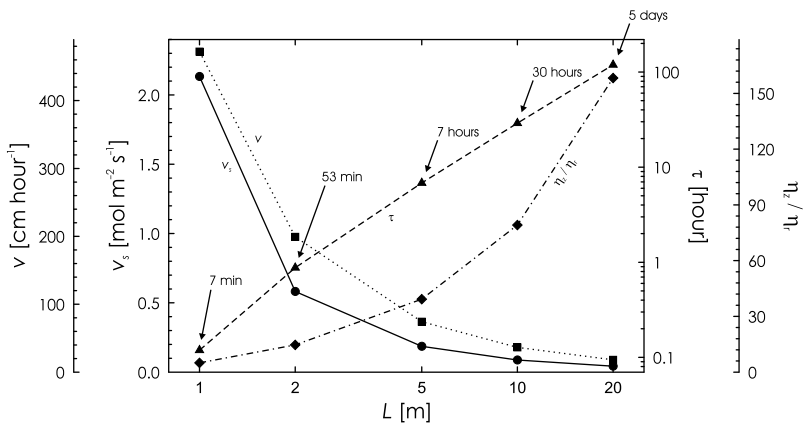

FIG. 5. Steady-state long-distance transport characteristics for five sieve tubes of varying lengths $L = 1$, 2, 5, 10, and 20 m. Each sieve tube has the same geometry as described in Section 3.1. Concentration is set to 1250 and 500 mol m^{-3} in the loading and unloading zones, respectively, while varying the loading rate to meet this condition in the loading zone (the unloading zone concentration is set by c^*). Shown are the sap velocity or flux density v (dotted line with squares), the sucrose flux density v_s (solid line with circles), the mean transit time of the system τ (dashed line with triangles), and the ratio of axial to membrane irreversible energy dissipation η_z/η_r (dashed–dotted line with diamonds). Sap flux density and sucrose flux density drop inversely with L, while the transit time increases roughly with the square of L. The dissipation ratio give an index of the strength of axial resistance relative to membrane resistance. In all simulations shown here, η_z/η_r is at least 4, suggesting that even at low sieve tube lengths, membrane conductance is only marginally limiting to transport.

tubes are capable of providing adequate assimilate transport between leaves and distant sink tissues. A number of different kinds of materials are transported in the phloem. If sucrose were the only solute, this would not be a problem, since it is stored all along the translocation pathway (Patrick *et al.*, 2001), buffering changes in the loading or unloading rate at the ends via temporary mobilization in the intermediate zone. Many substances, however, are not delivered as metabolic assimilates, but as molecular signals. Hormones are transported in the phloem (Ziegler, 1975), and their physiological efficacy may be contingent on their rapid translocation throughout the plant. Although we cannot say anything conclusive here about whether a 5 day transit time is prohibitively long, we can certainly say that transport will take far longer at greater distances and that plants with longer axes could be forced to lower their sieve plate resistance, or maintain shorter sieve tubes linked in series, or both.

Also shown in Fig. 5 is the ratio η_z/η_r of the irreversible energy dissipation rates of axial flow and radial membrane transport. In these simulations, this ratio is always significantly greater than unity (a minimum value of 5) indicating that axial resistance to transport dominates the flow regime.

3.2.2. *Loading Zone Sensitivity*

To test the transient, frequency-dependent behavior of the system at different values of L, we applied a small sinusoidal and diurnal impulse wave function in the unloading zone to these same steady-state simulations, such that

$$b_{unload}(t) = b_{unload}(0)\left[1 - \zeta \sin\left(\frac{2\pi t}{86\,400\,\mathrm{s}}\right)\right], \quad (25)$$

where $b_{unload}(0)$ equals minus the loading rate at all t, t is in seconds, and the denominator of 86 400 s sets the sine function to a diurnal cycle, with a drop in the unloading rate during the first half of the cycle, followed by a rise in the second half. ζ is the amplitude of the sine function, and is set arbitrarily by

$$\zeta = \frac{\pi(0.01)\sum_{i=1}^{N} C_i A_i \Delta z}{(86\,400\,\mathrm{s})\sum_{i=1}^{N(d/L)} B_i \Delta z}, \quad (26)$$

where the factor 0.01 in parentheses is the limit (1%) by which the change in unloading rate is allowed to alter the sucrose content of the model domain over half a day's time. The summation in the numerator gives the total sucrose content of the system, while that in the denominator gives the total loading rate. Here, ζ varied between 0.0003 at $L = 1\,\mathrm{m}$ and 0.312 at $L = 20\,\mathrm{m}$, roughly as a function of L^2.

The impulse function in eqn (25) was applied for 4 days, after which the variation in unloading rate, unloading zone sucrose concentration, loading zone sucrose concentration, and the phase shift ϕ between changes in c_{unload} and changes in c_{load} were determined (Fig. 6). The sensitivity of c_{load} to changes in c_{unload} (given as the ratio of their coefficients of variation), drops considerably as L increases, while the phase shift ϕ increases, from about 7 min at $L = 1\,\mathrm{m}$, to 3 hr at $L = 5\,\mathrm{m}$, to 16 hr at $L = 20\,\mathrm{m}$. Thus, not only are longer sieve tubes slow at delivering their assimilates to distant points in the plant, but they are considerably less sensitive to changes in supply or demand at one or the other ends of the tube.

Of particular interest given the recently intense work on identifying and characterizing membrane transporters in the phloem sieve element/companion cell complex (Patrick *et al.*, 2001) is that at very low L, total sieve tube concentration is extremely sensitive to small differentials between the loading and unloading rates (Fig. 6). Even the smallest increase or decrease in b (in this case, less than a tenth of a percent at $L = 1\,\mathrm{m}$) can lead rapidly to either feast or famine, a situation redolent of "the comatose patient and the hyperactive nurse" of van Bel *et al.* (2002), where the activity of the sieve element depends heavily on the participation of its companion cell.

4. Concluding Comments

The model presented here represents a significant technical improvement over previous

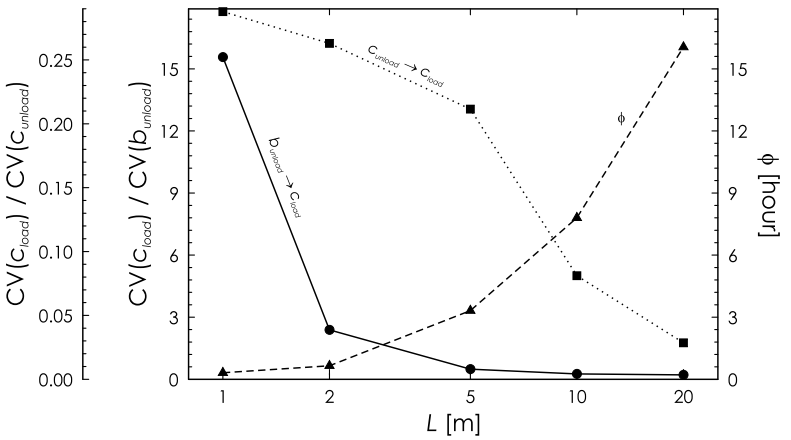

FIG. 6. Non-steady-state long-distance transport characteristics for five sieve tubes of varying length $L = 1, 2, 5, 10$, and 20 m, built on the steady-state results reported in Fig. 5. Here, the unloading zone of each tube was exposed to small, sinusoidal, diurnal fluctuations in unloading rate, while recording variation in time-dependent variation in the sucrose concentrations of the loading and unloading zones. Left axes: the ratio of the coefficient of variation (CV, standard deviation divided by the mean) of c_{load} the loading zone concentration to the CV of c_{unload} (dotted line with squares), and the ratio of the CV of c_{load} to the CV of the unloading rate b_{unload} (solid line with circles). Right axis: the phase shift ϕ (hr) between peak values of concentration in the unloading zone to peak values in the loading zone. In shorter sieve tubes, the loading zone concentration is very sensitive to changes in the unloading zone concentration, with very little phase shift, whereas in longer sieve tubes this sensitivity is largely lacking. Additionally, in shorter sieve tubes, the loading zone concentration is extremely sensitive to changes in loading and unloading rate.

models. The inclusion of wall elasticity, an improved formulation for sieve plate resistance, nonlinear viscosity and solute potential relations, and an improved numerical approach incorporating a modified Newton–Raphson iteration method and a slope-limiting TVD method for determining node boundary concentrations, make it available to test a number of hypotheses not previously explored in a modeling context. The simulation can handle sharp, fast-moving concentration fronts quite well at all spatial resolutions and without significant smearing (largely due to the inclusion of the TVD method), and it produces results that are qualitatively very similar to the results of previously developed numerical models (Tyree *et al.*, 1974; Goeschl *et al.*, 1976; Smith *et al.*, 1980).

The inclusion of wall elasticity has shown us that expandability of the sieve tube walls is probably of little biological significance in altering sieve tube conductivity. Because the sieve plates present most of the resistance to axial flow, an increase in lumen radius—though significantly increasing the conductance of the lumen itself—will have little effect on the overall conductivity of the sieve tube. This is counter to the suspicions of Lee (1981) and Sovonick-Dunford *et al.* (1982), who proposed that transient changes in lumen pressure could act to locally increase sieve tube conductance and increase the rate of flow.

The resistance to flow provided by the sieve plates is not trivial, even in the absence of occluding P-proteins. Ratios of axial to membrane irreversible energy dissipation strongly suggest that in all simulations the predominant resistance to flow is axial. Moreover, the geometry of the sieve tube was such that the sieve plates decreased the conductivity of the sieve tube by as much as 85%. We must therefore expect that in a number of cases, sieve tubes, depending on their internal anatomy, could be quite ineffective at transporting assimilates over long distances. Evolutionary changes in anatomy that might seem superficially to have the potential to increase axial conductance, such as an increase in sieve tube radius, which would have little effect in the presence of sieve plates, or an increase in sieve plate conductivity, which seems unlikely given the protective role of sieve plates against herbivores,

will not significantly improve the transport capacity of long sieve tubes. Other changes, such as the addition of osmotically active amine-nitrogen and electrolytes to the sieve sap, could increase transport rates to a point, but not enough to overcome the strong $1/L^2$ proportionality of transit time.

This model, like others before it, assumes that the only solute constituent of phloem sap is sucrose. The mathematical difficulties of including additional solutes are not insurmountable. However, our emphasis on sucrose is not due to a technical limitation but a pragmatic one: if the feasibility of OGPF can be shown with sucrose alone, additional solutes will only help its cause. To this day, no effort has been made to include other solutes in this kind of model—though some mention of an unpublished K^+ model was made by Komor *et al.* (1996). It is not entirely known how other solutes will affect transport, though it has long been suspected that they may play a crucial role. Lang (1983) hypothesized that potassium and its salts, which are far less viscous than sucrose, could significantly enhance OGPF. Potassium is a particularly strong candidate for supplemental osmotic control of phloem translocation. It is the dominant sieve tube cation (MacRobbie, 1971; Pate, 1975; Ziegler, 1975), it has high solute pressure at a relatively low viscosity (Hoad & Peel, 1965; Mengel & Haeder, 1977; Smith & Milburn, 1980a, b), and sucrose transport is limited in plants grown in K^+ limiting soil, even though there is no reduction in photosynthesis (Hartt, 1969; Mengel & Viro, 1974). Moreover, as noted by Lang (1983), sucrose transport rates are often better correlated with gradients in potassium concentration than with gradients in sucrose (Grange & Peel, 1978). Nevertheless, K^+ is known to be present in sieve sap at concentrations corresponding to no more than 3/4 the solute potential of sucrose (Lang, 1983). An increase in the driving gradient of as much as 75%—as such a K^+ concentration would amount to—could only increase the flow rate by that amount. Therefore, in the presence of potassium ions at these concentrations, transit times could be reduced by no more than 40%.

In fact, the best course for a plant faced with long transport distances seems to be a reduction in the length of the sieve tube, rather than any modification to the osmotic constituents of the sap. Instead of relying on a single osmotically isolated path from source to sink, the plant ought to rely on a set of such paths arranged in series. As seen in Section 3.2.1, transit time decreases with the inverse square of L. A halving of the transport distance would therefore mean a quartering of the transit time, and a quartering of the distance would reduce the transit time to 1/16th. It is not difficult to see, then, how two concatenated 10 m sieve tubes would have a composite transit time of only 1/2 that of a single 20 m sieve tube, and four 5 m sieve tubes only 1/4 that of a 20 m tube. Thus the transit time of a composite system would vary linearly with the inverse of L, rather than with its inverse square.

The advantage of a composite or "relay" (Lang, 1979; Aikman, 1980; Murphy & Aikman, 1989) system in plants is the balance struck between the stately elegance of OGPF and the precise control and increased speed afforded by intermediate active transport. The only disadvantage, aside from the cost of active loading, is that a reduction in L also makes sieve tube sucrose concentration considerably more sensitive to sudden changes or differentials between loading and unloading rates (as seen in Section 3.2.2). A low value of τ means that transport through the system is rapid relative to storage. Any change in b, therefore, at either end of the tube, could spell significant and rapid changes in concentration that only a very attentive companion cell could correct.

If active transport relays are present between axially adjoined sieve tubes, then the standard textbook depiction of phloem transport becomes untenable. In the textbooks, a single, osmotically isolated sieve tube is responsible for transport along the entire length of the plant. Solutes are brought to points in the plant where they are needed according to the differences in rate of consumption between those points, and no intermediate control is strictly necessary. However, if there is intermediate active transport between consecutive sieve tubes transport will be markedly faster, despite the metabolic cost of active transport and the unfortunate reduction

in elegance. That there is intermediate active transport is at least circumstantially supported by the presence of sucrose and water membrane transporters (Patrick *et al.*, 2001) throughout the plant. Passive loss and active loading of sucrose are known to occur everywhere (Komor *et al.*, 1996). Perhaps this "leak-pump" behavior of phloem tissue is not simply a matter of storage or assimilate supply to stem tissue, but additionally directed at transporting sucrose from one sieve tube to the next. Münch's vision of phloem transport would still be generally correct: demand for assimilates would continue as the ultimate determinant of solute partitioning, and OGPF would continue to be the principle means of moving solutes between sites of active transport, but the control of speed and direction would be proximally controlled at intermediate membrane boundaries. "Sink-strength" is then not only a misnomer (Minchin & Thorpe, 1993), but proximally incorrect, as well.

Unfortunately, this hypothesis is difficult to test directly. Little is known about the fine-scale anatomy of the phloem in different taxa; indeed, the values of β and k used here are just hopeful estimates. While plant physiologists and molecular biologists have done much in the last 15 years to clarify the mechanisms of loading and unloading in various plant tissues, little has been done to marry that information to what is known of phloem anatomy in wood and in other stem organ tissues. The hope with this model is that it will provide a good point of departure for further studies of transients in phloem transport. Future work will explore the functional limitations of phloem structural features (of those limited studies already published), provide better estimates of β across taxa and better estimates of resistance under particular geometries—such as those of conifers whose sieve cells are uniformly permeated by sieve pores, on lateral as well as transverse walls.

We wish to thank Maciej Zwieniecki, Alexander Cobb, Taylor Feild, Donald Fisher, Rachel Spicer, Lauren Sack, and James Rice for helpful input, and Howard Stone for exceedingly useful advise on how to handle the fluid mechanics of the sieve plate. We also wish to thank one anonymous reviewer. This research was supported by the Andrew W. Mellon Foundation.

REFERENCES

Aikman, D. P. (1980). Contractile proteins and hypotheses concerning their role in phloem transport. *Can. J. Bot.* **58,** 826–832.

Aikman, D. P. & Anderson, W. P. (1971). A quantitative investigation of a peristaltic model of phloem translocation. *Ann. Bot. London* **35,** 761–772.

Aronoff, S., Dainty, J., Gorham, P. R., Srivastava, L. M. & Swanson, C. A. (eds) (1975). *Phloem Transport*, 636pp. New York: Plenum Press.

Bouchard, C. & Grandjean, B. P. A. (1995). A neural network correlation for the variation of viscosity of sucrose aqueous solutions with temperature and concentration. *Lebensm. Wiss. Technol.* **28,** 157–159.

Canny, M. J. (1973). *Phloem Translocation*, 301pp. Cambridge: Cambridge University Press.

Canny, M. J. & Phillips, O. M. (1963). Quantitative aspects of a theory of translocation. *Ann. Bot. London* **27,** 379–402.

Celia, M. A., Bouloutas, E. T. & Zarba, R. L. (1990). A general mass-conservative numerical solution of the unsaturated flow equation. *Water Resour. Res.* **26,** 1483–1496.

Christy, A. L. & Ferrier, J. M. (1973). A mathematical treatment of Münch's pressure-flow hypothesis of phloem translocation. *Plant Physiol.* **52,** 531–538.

Christy, A. L. & Fisher, D. B. (1978). Kinetics of ^{14}C-photosynthate translocation in morning glory vines. *Plant Physiol.* **61,** 283–290.

Crafts, A. S. & Crisp, C. E. (1971). *Phloem Transport in Plants*, 481pp. San Francisco: W. H. Freeman and Co.

Cronshaw, J. (1975). P-proteins. In: *Phloem Transport* (Aronoff, S., Dainty, J., Gorham, P. R., Srivastava, L. M. & Swanson, C. A., eds), pp. 79–115. New York: Plenum Press.

Curtis, O. F. (1935). *The Translocation of Solutes in Plants*, 273pp. New York: McGraw-Hill.

Dagan, Z., Weinbaum, S. & Pfeffer, R. (1982). An infinite-series solution for the creeping motion through an orifice of finite length. *J. Fluid Mech.* **115,** 505–523.

Eckardt, N. A. (2001). A calcium-regulated gatekeeper in phloem sieve tubes. *Plant Cell* **13,** 989–992.

Ehlers, K., Knoblauch, M. & van Bel, A. J. E. (2000). Ultrastructural features of well-preserved and injured sieve elements: minute clamps keep the phloem transport conduits free for mass flow. *Protoplasma* **214,** 80–92.

Esau, K. (1969). *The Phloem. Handbuch der Pflanzenanatomie Histologie*, *Band V*, *Teil 2*, 505pp. Berlin, Stuttgart: Gebrüder Borntraeger.

Eschrich, W., Evert, R. F. & Young, J. H. (1972). Solution flow in tubular semipermeable membranes. *Planta* **107,** 279–300.

Eszterle, M. (1993). Molecular structure and specific volume of pure sucrose solutions. *Zuckerindustrie* **118,** 459–464.

Evert, R. F. (1982). Sieve-tube structure in relation to function. *BioScience* **32,** 789–795.

EWING, R. E. & WANG, H. (2001). A summary of numerical methods for time-dependent advection-dominated partial differential equations. *J. Comput. Appl. Math.* **128,** 423–445.

FARRAR, J. F. (1993). Sink strength: what is it and how do we measure it? *Plant Cell Environ.* **16,** 1013–1046.

FENSOM, D. S. (1981). Problems arising from a Münch-type pressure flow mechanism of sugar transport in phloem. *Can. J. Bot.* **59,** 425–432.

FERRIER, J. M. (1978). Further theoretical analysis of concentration–pressure–flux waves in phloem transport systems. *Can. J. Bot.* **56,** 1086–1090.

FERRIER, J. M. & CHRISTY, A. L. (1975). Time-dependent behavior of a mathematical model for Munch translocation: application to recovery from cold inhibition. *Plant Physiol.* **55,** 511–514.

FERRIER, J. M., TYREE, M. T. & CHRISTY, A. L. (1975). The theoretical time-dependent behavior of a Münch pressure-flow system: the effect of sinusoidal time variation in sucrose loading and water potential. *Can. J. Bot.* **53,** 1120–1127.

FISHER, D. B. (1970). Kinetics of C-14 translocation in soybean. *Plant Physiol.* **45,** 107–113.

FISHER, D. B. (1978). An evaluation of the Münch hypothesis for phloem transport in soybean. *Planta* **139,** 25–28.

FISHER, D. B., HOUSLEY, T. L. & CHRISTY, A. L. (1978). Source pool kinetics for ^{14}C-photosynthate translocation in morning glory and soybean. *Plant Physiol.* **61,** 291–295.

FRIED, J. J. (1975). *Groundwater Pollution: Theory, Methodology, Modelling and Practical Rules*, 330pp. New York: Elsevier.

GOESCHL, J. D. & MAGNUSON, C. E. (1986). Physiological implications of the Münch–Horwitz theory of phloem transport: effect of loading rates. *Plant Cell Environ.* **9,** 95–102.

GOESCHL, J. D., MAGNUSON, C. E., DEMICHELE, D. W. & SHARPE, P. J. H. (1976). Concentration-dependent unloading as a necessary assumption for a closed form mathematical model of osmotically driven pressure flow in phloem. *Plant Physiol.* **58,** 556–562.

GOODMAN, J. B. & LEVEQUE, R. J. (1988). A geometric approach to high resolution TVD schemes. *SIAM J. Numer. Anal.* **25,** 268–284.

GRANGE, R. I. & PEEL, A. J. (1978). Evidence for solution flow in the phloem of willow. *Planta* **138,** 15–23.

HARTT, C. E. (1969). Effect of potassium deficiency upon translocation of ^{14}C in attached blades and entire plants of sugarcane. *Plant Physiol.* **44,** 1461–1469.

HOAD, G. V. & PEEL, A. J. (1965). Studies on the movements of solutes between the sieve tubes and surrounding tissues in willow. I. Interference between solutes and rate of translocation measurements. *J. Exp. Bot.* **15,** 433–451.

HOCKING, P. J. (1980). The composition of phloem exudate and xylem sap from tree tobacco (*Nicotiana glauca* Grah.). *Ann. Bot. London* **45,** 633–643.

HORWITZ, L. (1958). Some simplified mathematical treatments of translocation in plants. *Plant Physiol.* **33,** 81–93.

ISTOK, J. (1989). *Groundwater Modeling by the Finite Element Method*, 495pp. Washington, DC: American Geophysical Union.

KAUFMANN, M. R. & KRAMER, P. J. (1967). Phloem water relations and translocation. *Plant Physiol.* **42,** 191–194.

KEDEM, O. & KATCHALSKY, A. (1958). Thermodynamic analysis of the permeability of biological membranes to non-electrolytes. *Biochim. Biophys. Acta.* **27,** 229–246.

KNOBLAUCH, M. & VAN BEL, A. J. E. (1998). Sieve tubes in action. *Plant Cell* **10,** 35–50.

KNOBLAUCH, M., PETERS, W. S., EHLERS, K. & VAN BEL, A. J. E. (2001). Reversible calcium-regulated stopcocks in legume sieve tubes. *Plant Cell* **13,** 1221–1230.

KÖCKENBERGER, W., POPE, J. M., XIA, Y., JEFFREY, K. R., KOMOR, E. & CALLAGHAN, P. T. (1997). A non-invasive measurement of phloem and xylem water flow in castor bean seedlings by nuclear magnetic resonance microimaging. *Planta* **201,** 53–63.

KOMOR, E., ORLICH, G., WEIG, A. & KÖCKENBERGER, W. (1996). Phloem loading—not metaphysical, only complex: towards a unified model of phloem loading. *J. Exp. Bot.* **47,** 1155–1164.

LANG, A. (1978). A model of mass flow in the phloem. *Aust. J. Plant Physiol.* **5,** 535–546.

LANG, A. (1979). A relay mechanism for phloem translocation. *Ann. Bot. London* **44,** 141–145.

LANG, A. (1983). Turgor-regulated translocation. *Plant Cell Environ.* **6,** 683–689.

LEE, D. R. (1981). Elasticity of phloem tissues. *J. Exp. Bot.* **32,** 251–260.

MACROBBIE, E. A. C. (1971). Phloem translocation. Facts and mechanisms: a comparative survey. *Biol. Rev.* **46,** 428–481.

MAGNUSON, C. E., GOESCHL, J. D., SHARPE, P. J. H. & DEMICHELE, D. W. (1979). Consequences of insufficient equations in models of the Münch hypothesis of phloem transport. *Plant Cell Environ.* **2,** 181–188.

MAGNUSON, C. E., GOESCHL, J. D. & FARES, Y. (1986). Experimental tests of the Münch-Horwitz theory of phloem transport: effects of loading rates. *Plant Cell Environ.* **9,** 103–109.

MENGEL, K. & HAEDER, H. E. (1977). Effect of potassium supply on the rate of phloem sap exudation and the composition of the phloem sap of *Ricinus communis*. *Plant Physiol.* **59,** 282–284.

MENGEL, K. & VIRO, M. (1974). Effect of potassium supply on the transport of photosynthates to the fruits of tomatoes (*Lycopersicon esculentum*). *Physiol. Plantarum* **30,** 295–300.

MICHEL, B. E. (1972). Solute potentials of sucrose solutions. *Plant Physiol.* **50,** 196–198.

MILBURN, J. A. (1975). Pressure flow. In: *Encyclopedia of Plant Physiology, Transport in Plants I, Phloem Transport* (Zimmermann, M. H. & Milburn, J. A., eds), pp. 328–353. New York: Springer-Verlag.

MILLY, P. C. D. (1988). Advances in modeling of water in the unsaturated zone. *Transport Porous Medium* **3,** 491–514.

MINCHIN, P. E. H. & THORPE, M. R. (1993). Sink strength—a misnomer, and best forgotten. *Plant Cell Environ.* **16,** 1039–1040.

MINCHIN, P. E. H. & THORPE, M. R. (1996). What determines carbon partitioning between competing sinks? *J. Exp. Bot.* **47,** 1293–1296.

MINCHIN, P. E. H., THORPE, M. R. & FARRAR, J. F. (1993). A simple mechanistic model of phloem transport which explains sink priority. *J. Exp. Bot.* **44,** 947–955.

MÜNCH, E. (1926). Über Dynamik der Saftströmungen. *Ber. Deut. Bot. Ges.* **44,** 68–71.
MÜNCH, E. (1927). Versuche über den Saftkreislauf. *Ber. Deut. Bot. Ges.* **45,** 340–356.
MÜNCH, E. (1930). *Die Stoffbewegungen in der Pflanze*. Jena: Gustav Fischer.
MURPHY, R. (1989a). Water flow across the sieve-tube boundary: estimating turgor and some implications for phloem loading and unloading. I. Theory. *Ann. Bot. London* **63,** 541–549.
MURPHY, R. (1989b). Water flow across the sieve-tube boundary: estimating turgor and some implications for phloem loading and unloading. II. Phloem in the stem. *Ann. Bot.London* **63,** 551–559.
MURPHY, R. (1989c). Water flow across the sieve-tube boundary: estimating turgor and some implications for phloem loading and unloading. III. Phloem in the leaf. *Ann. Bot.London* **63,** 561–570.
MURPHY, R. (1989d). Water flow across the sieve-tube boundary: estimating turgor and some implications for phloem loading and unloading. IV. Root tips and seed coats. *Ann. Bot.London* **63,** 571–579.
MURPHY, R. & AIKMAN, D. P. (1989). An investigation of the relay hypothesis of phloem transport in *Ricinus communis* L. *J. Exp. Bot.* **40,** 1079–1088.
NIELSEN, D. R., VAN GENUCHTEN, M. T. & BIGGAR, J. W. (1986). Water flow and solute transport processes in the unsaturated zone. *Water Resour. Res.* **22,** 89S–108S.
OPARKA, K. J. (1990). What is phloem unloading? *Plant Physiol.* **94,** 393–396.
OPARKA, K. J. & CRUZ, S. S. (2000). The great escape: phloem transport and unloading of macromolecules. *Annu. Rev. Plant Phys.* **51,** 323–347.
OPARKA, K. J. & TURGEON, R. (1999). Sieve elements and companion cells–traffic control centers of the phloem. *Plant Cell* **11,** 739–750.
PASSIOURA, J. B. & ASHFORD, A. E. (1974). Rapid translocation in the phloem of wheat roots. *Aust. J. Plant Physiol.* **1,** 521–527.
PATE, J. S. (1975). Exchange of solutes between phloem and xylem and circulation in the whole plant. In: *Encyclopedia of Plant Physiology, Transport in Plants I, Phloem Transport* (Zimmermann, M. H. & Milburn, J. A. eds), pp. 451–473. New York: Springer-Verlag.
PATRICK, J. W. (1997). Phloem unloading: sieve element unloading and post-sieve element transport. *Annu. Rev. Plant Phys.* **48,** 191–222.
PATRICK, J. W., ZHANG, W., TYERMAN, S. D., OFFLER, C. E. & WALKER, N. A. (2001). Role of membrane transport in phloem translocation of assimilates and water. *Aust. J. Plant Physiol.* **28,** 695–707.
PHILLIPS, R. J. & DUNGAN, S. R. (1993). Asymptotic analysis of flow in sieve tubes with semi-permeable walls. *J. theor. Biol.* **162,** 465–485, doi:10.1006/jtbi.1993.1100.
ROSS, S. M. & TYREE, M. T. (1980). A reanalysis of the kinetics of ^{14}C photosynthate translocation in morning glory vines. *Ann. Bot. London* **46,** 727–738.
SHEEHY, J. E., MITCHELL, P. L., DURAND, J. L., GASTAL, F. & WOODWARD, F. I. (1995). Calculation of translocation coefficients from phloem anatomy for use in crop models. *Ann. Bot.London* **76,** 263–269.
SMITH, J. A. C. & MILBURN, J. A. (1980a). Osmoregulation and the control of phloem-sap composition in *Ricinus communis* L. *Planta* **148,** 28–34.
SMITH, J. A. C. & MILBURN, J. A. (1980b). Phloem transport, solute flux and the kinetics of sap exudation in *Ricinus communis* L. *Planta* **148,** 35–41.
SMITH, K. C., MAGNUSON, C. E., GOESCHL, J. D. & DEMICHELE, D. W. (1980). A time-dependent mathematical expression of the Münch hypothesis of phloem transport. *J. theor. Biol.* **86,** 493–505.
SOVONICK-DUNFORD, S., Lee, D. R. & ZIMMERMANN, M. H. (1981). Direct and indirect measurements of phloem turgor pressure in white ash. *Plant Physiol.* **68,** 121–126.
SOVONICK-DUNFORD, S., FERRIER, J. M. & DAINTY, J. (1982). Water-relations parameters of phloem. Determinations of volumetric elastic modulus and membrane conductivity using an applied force method and shrinkage and swelling of tissues in solutions at differing osmotic pressure. *Ann. Bot. London* **51,** 27–37.
TAYLOR, G. (1954). Conditions under which dispersion of a solute in a stream of solvent can be used to measure molecular diffusion. *Proc. R. Soc. London Ser. A* **225,** 473–477.
THAINE, R. (1969). Movement of sugars through plants by cytoplasmic pumping. *Nature* **222,** 873–875.
TURGEON, R. & MEDVILLE, R. (1998). The absence of phloem loading in willow leaves. *Proc. Natl Acad. Sci. U.S.A.* **95,** 12055–12060.
TYREE, M. T. (1970). The symplast concept: a general theory of symplastic transport according to the thermodynamics of irreversible processes. *J. theor. Biol.* **26,** 181–214.
TYREE, M. T., CHRISTY, A. L. & FERRIER, J. M. (1974). A simpler iterative steady state solution of Münch pressure-flow systems applied to long and short translocation paths. *Plant Physiol.* **54,** 589–600.
VAN BEL, A. J. E. (1993). Strategies of phloem loading. *Annu. Rev. Plant Phys.* **44,** 253–281.
VAN BEL, A. J. E. & GAMALEI, Y. V. (1992). Ecophysiology of phloem loading in source leaves. *Plant Cell Environ.* **15,** 265–270.
VAN BEL, A. J. E., EHLERS, K. & KNOBLAUCH, M. (2002). Sieve elements caught in the act. *Trends Plant Sci.* **7,** 126–132.
WANG, H. F. & ANDERSON, M. P. (1982). *Introduction to Groundwater Modeling: Finite Difference and Finite Element Methods*, 237pp. New York: W. H. Freeman and Co.
WARDLAW, I. F. & PASSIOURA, J. B., (eds) (1976). *Transport and Transfer Processes in Plants*, 484pp. New York: Academic Press.
WEATHERLEY, P. E. & JOHNSON, R. P. C. (1968). The form and function of the sieve tube: a problem in reconciliation. *Int. Rev. Cytol.* **24,** 149–192.
WILCOX, D. C. (1997). *Basic Fluid Mechanics*, 741pp. La Cañada, California: DCW Industries, Inc.
WU, H.-I., SPENCE, R. D., SHARPE, P. J. H. & GOESCHL, J. D. (1985). Cell wall elasticity: I. A critique of the bulk elastic modulus approach and an analysis using polymer elastic principles. *Plant Cell Environ.* **8,** 563–570.
YOUNG, J. H., EVERT, R. F. & ESCHRICH, W. (1973). On the volume-flow mechanism of phloem transport. *Planta* **113,** 355–366.
ZIEGLER, H. (1975). Nature of transported substances. In: *Encyclopedia of Plant Physiology, Transport in Plants I, Phloem Transport* (Zimmermann, M. H. & Milburn, J. A. eds), pp. 59–100. New York: Springer-Verlag.

ZIMMERMANN, M. H. & BROWN, C. L. (1980). *Trees, Structure and Function*. New York: Springer-Verlag.
ZIMMERMANN, M. H. & MILBURN, J. A. (eds) (1975). *Encyclopedia of Plant Physiology, Transport in Plants I, Phloem Transport*, 535pp. New York: Springer-Verlag.
ZIMMERMANN, M. H. & ZIEGLER, H. (1975). Appendix III: list of sugars and sugar alcohols in sieve-tube exudates. In: *Encyclopedia of Plant Physiology*, *Transport in Plants I, Phloem Transport* (Zimmermann, M. H. & Milburn, J. A. eds), pp. 480–503. New York: Springer-Verlag.

Appendix A

A Modeling History of Osmotically Generated Pressure Flow

The first proposal of what is today known as the OGPF hypothesis was articulated by Ernst Münch to a meeting of the Deutsche Botanische Gesellschaft in February, 1926, as the "Dynamics of Sap Flow" (Münch, 1926). The proposal was followed by a more complete treatment of the hypothesis, including both physical and physiological experiments, which described how a

> local gradient in osmotic pressure, which develops by assimilation [*via photosynthesis*] or conversion from metabolically stored materials at one end of the gradient, and by consumption or metabolic storage of that assimilate at the other…produces pressure streams in the cell sap that automatically lead the necessary materials to where they are needed in proportion to their production and consumption (Münch, 1927, translation MVT).

Münch's system was both simple and elegant, and required only that the phloem transport pathway—or any osmotically isolated intercellular pathway—be of sufficiently low resistance to accommodate measured flow rates. Yet, despite its elegance, initial support for the OGPF hypothesis in the phloem was limited. Direct measurements supporting the existence of the necessary osmotic gradients were lacking, and it was generally believed that the sieve plates were blocked by P-proteins (Curtis, 1935; Canny & Phillips, 1963; Thaine, 1969; Aikman & Anderson, 1971; Canny, 1973; Fensom, 1981), a set of plastid-bound proteins in the cell lumen (Cronshaw, 1975) that upon damage expand and block the flow of sap through the sieve plates (Esau, 1969; Crafts & Crisp, 1971; Knoblauch & van Bel, 1998; Knoblauch *et al*., 2001). Normal methods of fixation for sectioning can activate the release of P-proteins, a fact of which if ignorant could lead to the belief that sieve plates are normally blocked. However, with careful handling, it is possible to prevent the wounding response (Evert, 1982; Ehlers *et al*., 2000), and today good evidence, both structural and physiological, supports the conclusion that sieve pores are free from obstruction under normal conditions (Knoblauch & van Bel, 1998). In addition, a variety of empirical approaches, including psychrometry (Kaufmann & Kramer, 1967; Sovonick-Dunford *et al*., 1981), radioactive tracer kinetics (Fisher, 1970; Christy & Fisher, 1978; Fisher *et al*., 1978; Ross & Tyree, 1980), negative staining (Fisher, 1978), and mass balance (Passioura & Ashford, 1974), have provided evidence for flow rates and osmotic pressure gradients commensurate with some of the predictions of the OGPF hypothesis.

A series of phloem transport models have been published over the last 40 years. Because the work presented here purports to improve on these models, a brief discussion of their history is in order, and will now follow. For a discussion of other phloem transport hypotheses, such as cytoplasmic streaming, electro-osmosis, particle streaming, and surface flow, see reviews in the edited volumes by Aronoff *et al*. (1975), Zimmermann & Milburn (1975), and Wardlaw & Passioura (1976). We give a summary of the relevant OGPF models in Table 1.

A.1. EARLY MODELING EFFORTS

The first mathematical analysis of Münch's OGPF hypothesis was presented by Horwitz (1958) in a discussion of the theoretical implications of radioactive tracer studies of translocation. Horwitz presented a complete system of differential equations for the unloading of a radioactive tracer along the transport pathway of the sieve tube, and concluded that mass flow systems such as described by the OGPF hypothesis are in close agreement with the available radio-decay data. However, as anything beyond a test of empirical data, his equations were

insufficient, since a complete model of the dynamics of pressure flow would require that the non-zero volume of sucrose itself be included, an issue ignored until the work of Christy & Ferrier (1973). Omitting $\overline{V_s}$ can lead to underestimates of the velocity as high as 25%.

Horwitz also justified the use of the Hagen–Poiseuille flow relation for the pressure gradient along the sieve tube and through sieve plates. He found that despite the large momentum changes attendant in sieve tube sap around and through the sieve plates, viscous effects are still dominant, with flow linearly proportional to the pressure drop, albeit with a slightly lower conductance than in a sieve plate free system. He also concluded that the changes in momentum incurred by the flux of water across the plasma membrane are sufficiently small to be ignored—not surprising given that characteristic Reynolds numbers in sieve tubes are in the range of 10^{-2}–10^{-3}. These conclusions, since they are important to the thermodynamic validity of the OGPF hypothesis, are further discussed in Appendix B of this paper.

Work by Eschrich *et al.* (1972) and Young *et al.* (1973) continued the mathematical analysis of the Münch flow system using a physical model made of dialysis tubing. Their work was a technical advance over the work of Horwitz (1958) in its delivery of a more rigorous presentation of the non-equilibrium thermodynamics of membrane transport. However, their formulation lacked a closed-form solution of solute concentration (it was prescribed arbitrarily), a realistic set of solute potential and viscosity curves, as well as a non-zero partial volume for sucrose.

A.2. MECHANISTICALLY COMPLETE MODELS

Mathematical analysis of the pressure-flow hypothesis made a qualitative leap forward with the models of Christy, Ferrier, and Tyree (Christy & Ferrier, 1973; Tyree *et al.*, 1974; Ferrier & Christy, 1975; Ferrier *et al.*, 1975; Ferrier, 1978). The system of equations they used was complete and allowed for closed-form solutions of solute concentration throughout the sieve tube, and was the first to account for the volumetric contribution of sucrose. Of these models, that of Ferrier *et al.* (1975) was the first to include concentration-dependent changes in viscosity and time-dependent changes in sucrose concentration as a function of loading rate and the apoplastic water potential—that is, it was the first non-steady-state model. Given the limited computing power available at the time, they employed numerical techniques that could be considered crude by today's standards. Especially problematic is their use of the upstream node's concentration to set the concentration of the node boundaries for internode flow, an approximation that can lead to significant solute smearing and an overestimate of the flux density of sucrose transport at a given loading rate, a problem which we fix with the slope-limiting total variation diminishing method. Nevertheless, their steady-state work confirmed the theoretical feasibility of long-distance transport (>50 m)—although it would be restricted to drastically reduced rates of flow—but warned of the danger of expecting long transport pathways to operate near steady state. As have many modelers since, Ferrier *et al.* (1975) employed a linear relationship between solute potential and sucrose concentration, dramatically underestimating solute potential at high concentrations (e.g. by 25% at 900 mol sucrose m^{-3} and 20°C), even though more accurate empirical relations for solute potential had been available for some time (Michel, 1972). Indeed, all models developed thus far (except the one presented in this work) have used the simple $-\Re Tc$ van't Hoff relation, valid only for small solute concentrations (Table 1).

Lang (1978) presented a steady-state model that tested the relative contributions of radial vs. axial flow resistance to the dynamics of the system. His system of equations was complete (though it lacked a sucrose volumetric term) and included an explicitly stated function of the dependence of dynamic viscosity on sucrose concentration. Lang (1978) also explored the importance of the relative osmotic strength of various carbohydrates with respect to their viscosity to determine the "ideal" solute concentrations for each.

Goeschl *et al.* (1976) and Magnuson *et al.* (1979) pointed out in response to earlier work by Christy & Ferrier (1973) that

to obtain a closed-form solution of solute transport in the phloem it was necessary to provide explicit, concentration-dependent functions of phloem unloading. Unless the solute flux density along the length of the sieve tube were prescribed—as done by Lang (1978), who used a flow boundary condition at one end of the tube—the concentration profile at steady state would not be unique. In response to the non-uniqueness problem, Goeschl *et al.* (1976) suggested a number of different functional forms for sucrose unloading, ranging from linear functions to Michaelis–Menten saturable kinetics.

Smith *et al.* (1980) introduced time-dependent properties to the model of Goeschl *et al.* (1976), developing a non-steady-state model of phloem transport, the first since that of Ferrier *et al.* (1975). Using a Newton–Raphson time-stepping method, Smith *et al.* (1980) dramatically improved non-steady-state phloem modeling over that of Ferrier *et al.* (1975) and Ferrier (1978). The steady-state results of their non-steady-state model agreed well with the steady-state results of Goeschl *et al.* (1976), on whose equations their model was based. Moreover, the steady-state results of Smith *et al.* (1980) were qualitatively identical to those of Christy & Ferrier (1973) and Tyree *et al.* (1974). Unfortunately, given the limited computing power available at the time, the spatial and temporal resolution of their non-steady-state approximation was low, making a thorough analysis of long-distance transport difficult.

A.3. LATER REFINEMENTS

A number of refinements to models of long-distance phloem transport have been made since the early 1980s. The theoretical implications of solution transport through the plasmodesmata connecting the sieve elements with their neighboring companion cells were first addressed in the late 1980s (Murphy, 1989a–d). By incorporating what was known of phloem plasmodesmatal transport, Murphy determined that the rate of sucrose unloading in trees across the sieve tube plasma membrane could be no more than 50 nmol (m^2 membrane area)$^{-1}$ s^{-1}, while over short distances the unloading rate could be as high as 100 nmol (m^2 membrane area)$^{-1}$ s^{-1}. (It should be noted that in this work rates of loading and unloading are typically at least one order of magnitude higher than this.) He also showed that the pressure flow of solution between the sieve elements and companion cells must be accounted for when calculating sieve tube pressure gradients from measurements, and that apoplastic loading of sucrose is more likely than loading via plasmodesmata. His approach was analytical and steady state, with the major contribution being a subtler grasp of the relationship of transport theory to measurement given the complexity of the plasmodesmata, rather than an advancement of the modeling of long-distance phloem transport. Plasmodesmatal kinetics in the loading and unloading of sucrose in the phloem is not germane to the essential biophysical questions of long-distance transport asked in this work. It is taken for granted here that sucrose is loaded and unloaded in some unspecified fashion, and that for our purposes arbitrarily prescribed functions describing those processes are sufficient.

Phillips & Dungan (1993) presented an analytical approach to steady-state phloem transport. Their solution was robust, but lacked the power that an equivalent numerical model would possess, and few of their claims that their work is mathematically more rigorous than previous efforts can be substantiated in their results. The conclusions that Phillips & Dungan (1993) make using a sophisticated solution of the Navier–Stokes equation (being a more general case of the Hagen–Poiseuille relation) are identical to those of the models they cite as incorrectly incorporating Hagen–Poiseuille flow: that as pressure drops in the sieve tube with distance, inward radial membrane flow will increase in magnitude, causing a further increase in velocity, an additional pressure drop, and dilution. As many theoretical studies (Eschrich *et al.*, 1972) have reported, a change in pressure gradient due to sucrose dilution and flow divergence is to be expected. Moreover, Phillips & Dungan (1993) incorrectly state their case when they say that other models globally apply the Hagen–Poiseuille flow relation to the entire sieve tube. In fact, these other models apply the Hagen–Poiseuille flow relation locally, and explicitly

include wall flow, producing the same sap acceleration that Phillips & Dungan (1993) claim can be achieved in no other way but through the use of the Navier–Stokes equation.

To our knowledge, no analytically complete model of the long-distance component of phloem transport has been published since 1993. A number of models have been developed to, explain sink priority in whole-plant translocation (see Minchin *et al.*, 1993, for example and references) or to derive translocation coefficients for use in crop models (Sheehy *et al.*, 1995), but these make simplifying assumptions that can eliminate their usefulness in detailed analyses of translocation, and it is not clear that we know enough about what kinds of resistances are attendant in the sieve tubes of tall or short plants to make meaningful, yet general, predictions for agricultural systems. In addition, although two nominally non-steady-state models have been developed (i.e. by Ferrier *et al.*, 1975; Smith *et al.*, 1980), neither of these models is available, neither includes the effects of the non-linear relationship of concentration on solute potential, and neither includes the elastic properties of phloem tissue. These deficiencies are addressed in this work.

Appendix B

Applicability of the Hagen–Poiseuille Flow Relation to Sieve Elements and Sieve Pores

Axial transport in this model was calculated assuming that flow rate was linearly proportional to the axial pressure gradient according to the Hagen–Poiseuille relation. For this assumption to be justified, a number of conditions must be met, namely that inertial transfer due to membrane transport and gravity have no significant effect on the pressure gradient, that a parabolic velocity profile is fully developed throughout each sieve element, and that the radial distribution of solute in the sieve tube is homogeneous (the justification for this will be given in the next section). Some confusion has arisen over the applicability of the Hagen–Poiseuille relation, as discussed in the previous section. Phillips & Dungan (1993) argue that the relation is not applicable to cases of flow in a porous tube, citing Christy & Ferrier(1973), Tyree *et al.* (1974) and Goeschl & Magnuson (1986) as cases where it has been incorrectly applied. However, while it is true that Hagen–Poiseuille flow does not on its own account for the changes in axial pressure gradient observed in the sieve tube in modeling studies, it does account, to a very good approximation, for the local conductivity of the sieve tube, as long as radial transport is explicitly included. The following section will justify the use of Hagen–Poiseuille flow as a very good approximation of *local* axial conductivity.

Phloem transport is characterized by low Reynolds numbers ($Re \ll 1$), and is therefore dominated by viscous effects. This can be shown directly by calculating the relative contribution to the pressure gradient of viscous forces on the one hand and the transfer of momentum via radial membrane flux on the other. These two components are, following Horwitz (1958):

$$\frac{\mathrm{d}p}{\mathrm{d}z} = -\frac{av}{k} - 2\rho v \frac{\mathrm{d}v}{\mathrm{d}z}, \qquad \text{(B.1)}$$

where the second term on the right-hand side is the inertial contribution. Using data for the steady state from Fig. 3, where v is approximately $2.4 \times 10^{-4}\,\mathrm{m\,s^{-1}}$, k is $1.4 \times 10^{-13}\,\mathrm{m^4\,s^{-1}\,MPa^{-1}}$, ρ is $1.1 \times 10^{3}\,\mathrm{kg\,m^{-3}}$, and the maximum value of $\mathrm{d}v/\mathrm{d}z$ is $7.8 \times 10^{-4}\,\mathrm{s^{-1}}$, the viscous contribution $-0.35\,\mathrm{MPa\,m^{-1}}$) is at least 800 times greater than the inertial contribution ($-4.1 \times 10^{-4}\,\mathrm{MPa\,m^{-1}}$). Thus, not only can the inertial components of the Navier–Stokes equation be neglected, but relative to viscous forces, radial flow will transfer very little momentum—and very little volume—to the sieve tube sap.

For Hagen–Poiseuille flow to be applicable, it must also be the case that the radial parabolic velocity profile be fully developed throughout the sieve element. Only near the sieve plate boundary is this assumption in danger, where the change in geometrical configuration as the sap flows through the sieve plate homogenizes the radial distribution of axial velocities. However, at these values of Re ($\ll 1$), we can expect Hagen–Poiseuille flow to become fully developed within less than 10% of the radius of the tube, or

within less than 0.3% of the total length of the sieve element (Wilcox, 1997, p. 214). Should this error seem too great, consider that any errors introduced by unjustifiably assuming fully developed flow will be swamped by the far greater resistance imposed by the sieve plates.

The gravitational component of transport can also be ignored, not because it is negligibly small—though it is small—but because of the phloem's close anatomical association with the xylem, the sap of which is subject to the same gravitational forces. Insofar as the densities of the two saps are the same (phloem sap density is only about 10% greater than that of the xylem), and assuming that the water transport between the xylem and phloem is sufficiently rapid (that is, that water potential in the sieve tube lumen is approximately that of the apoplast, and that the water potential of the apoplast is the same as in the adjacent xylem vessels), then the standing pressure gradient in the xylem will cancel the standing gradient in the phloem (Milburn, 1975). This is fortunate, since seldom is every part of a tree oriented strictly vertically. If we were required to account for the change in gravitational potential, we would also have to account for branch orientation. In any event, typical pressure gradients in the phloem (~ 0.4 MPa m^{-1} in Fig. 3) are much greater than the 0.01 MPa m^{-1} standing gradient imposed by gravity.

In previous work (Tyree *et al.*, 1974; Goeschl *et al.*, 1976), the hydraulic conductivity of the sieve plates was calculated as though it were a set of parallel pipes, connecting one sieve element to the next. Flow through each of the pores was assumed to be Hagen–Poiseuille, and since the pressure difference across the sieve plate was assumed to be constant for all pores, the flow rate was the same through each. While providing a good approximation, the "parallel-pipe" model is insufficient in cases where the pores are very short, when the resistance imposed by the reduction (and subsequent increase) in the aspect ratio of the flow path as the fluid passes through the sieve plate becomes significant. Previous authors, who assumed strict adherence to Hagen–Poiseuille flow (Tyree *et al.*, 1974; Goeschl *et al.*, 1976), calculated the pressure drop across a pore Δp_{pore} as

$$\Delta p_{pore} = -\frac{8\mu l_p}{\pi r_p^4} j_p, \tag{B.2}$$

where Δp_{pore} is everywhere the same across a single plate, and j_p is the mass flow of phloem solution through a single sieve pore. However, by inspection, eqn (B.2) seems to indicate that the pressure drop across the sieve plate drops to zero as the pore length became infinitesimally small. A solution to this problem is presented by Dagan *et al.* (1982), who found that the pressure drop due to Hagen–Poiseuille flow through a finite-length pore can be given by the standard formulation given in eqn (B.2), plus an additional pressure drop given by Sampson (1891; cited by Dagan *et al.*, 1982) for pores set in infinitesimally thin, infinite-extent planes. The Sampson pressure drop across an infinitesimally thin sieve pore $\Delta p_{pore,\ Sampson}$ is (Dagan *et al.*, 1982):

$$\Delta p_{pore,\ Sampson} = -\frac{3\mu}{r_p^3} j_p, \tag{B.3}$$

which does not drop to zero at zero pore length. The total pressure drop across the pore Δp^*_{pore} is then

$$\Delta p^*_{pore} = -\left[\frac{8l_p + 3\pi r_p}{8l_p}\right]\left(\frac{8\mu l_p}{\pi r_p^4}\right) j_p, \tag{B.4}$$

where φ (dimensionless) is the Sampson factor and is equal to the inverse of the quantity in brackets:

$$\varphi = \frac{8l_p}{8l_p + 3\pi r_p}, \tag{B.5}$$

such that

$$\Delta p^*_{pore} = -\frac{1}{\varphi}\left(\frac{8\mu l_p}{\pi r_p^4}\right) j_p. \tag{B.6}$$

Here, in the limiting case that l_p approaches zero, φ will approach zero, and eqn (B.6) will reduce to (B.3).

Equation (B.6) can be rewritten for flow, j, across the entire sieve plate:

$$\Delta p^*_{pore} = -\frac{1}{\varphi N_p}\left(\frac{8\mu l_p}{\pi r_p^4}\right) j, \tag{B.7}$$

where N_p is the number of pores contained in a single sieve plate. The axial pressure drop along a single sieve tube lumen is given by

$$\Delta p_{lumen} = -\frac{8\mu(l - l_p)}{\pi r^4} j, \tag{B.8}$$

where the quantity $(l - l_p)$ is the distance between consecutive sieve plates. Under mass conservation, j for the sieve plate should equal j for the sieve tube lumen, such that the total pressure drop across a single lumen and one adjacent sieve plate is given by

$$\Delta p_T = -\frac{8\mu}{\pi}\left[\frac{l_p}{\varphi N_p r_p^4} + \frac{(l - l_p)}{r^4}\right] j. \tag{B.9}$$

From this, given that

$$j = -k\frac{\Delta p_T}{l}, \tag{B.10}$$

where k is the combined conductivity of the lumen plus sieve plate, we arrive at a formula for k that takes into account the Hagen–Poiseuille pressure drop of both the lumen and sieve pores, plus the pressure drop due to the Sampson result:

$$k = \left[\frac{\varphi N_p r_p^4 l}{\varphi N_p r_p^4 (l - l_p) + r^4 l_p}\right]\frac{\pi r^4}{8\mu} \tag{B.11}$$

Setting the quantity in brackets equal to β, sieve tube conductivity is given by

$$k = \beta\frac{\pi r^4}{8\mu}, \tag{B.12}$$

where

$$\beta = \frac{\alpha\varphi r_p^2 l}{\alpha\varphi r_p^2 (l - l_p) + r^2 l_p}, \tag{B.13}$$

and α is the fraction of the sieve plate area composed of sieve pore area, such that

$$\alpha = N_p\frac{\pi r_p^2}{\pi r^2} = N_p\frac{r_p^2}{r^2}. \tag{B.14}$$

Note that we assume the radius of the sieve pores to remain constant during sieve element expansion.

Under the sieve tube geometry employed here ($r = 7.5\,\mu m$, $l = 250\,\mu m$, $l_p = 0.5\,\mu m$, $r_p = 0.23\,\mu m$, and $\alpha = 0.5$) β is approximately 0.132. When the sieve pores are long relative to their diameter (i.e., when $l_p \gg r_p$), the Sampson factor approaches unity and eqn (B.13) approaches the standard solution as used by other authors. As pore length decreases, however, the Sampson factor becomes important (i.e. it approaches zero), where the limit of β as l_p approaches zero is

$$\lim_{l_p \to 0} \beta = \frac{8\alpha r^2 r_p l}{8\alpha r^2 r_p l + 3\pi r^4}. \tag{B.15}$$

The introduction of the Sampson factor ensures that even if the pores are very short (i.e., $l_p \ll r_p$), there is always some, and in this case quite considerable, resistance to flow.

The Sampson resistance term assumes that the zero-length pore it treats is embedded in zero-thickness plane of infinite extent. Here, of course, we are dealing with pores that are considerably more densely packed. However, to a first-order approximation, its inclusion is acceptable (Howard A. Stone, Division of Engineering and Applied Sciences, Harvard University, pers. comm.), and clearly an improvement over previous sieve plate impedance formulations.

Appendix C

Molecular Diffusion and the Axial and Radial Transport of Solutes

The current construction of the solute conservation eqn (13) assumes that axial diffusion and dispersion are negligible relative to axial convection, and that radial diffusion is sufficiently fast to ensure the solute's radial homogeneity. If the former were not the case, then terms for axial diffusion would have to be included, arguably increasing the complexity of the solution. If the latter were not the case, and a significant radial profile in sucrose could be expected, then there would be a non-uniform distribution of viscosity, and the Hagen–Poiseuille relation would not strictly hold (though it could represent a good first-order

approximation). Radially heterogeneous solute concentrations would also invalidate eqn (8), which relies on the assumption that the mean radial concentration of sucrose is the same as the concentration at the wall boundary.

Had we included axial diffusion, axial solute flow would have taken the following form:

$$j_s = cj - aD_m \frac{\partial c}{\partial z}. \tag{C.1}$$

where D_m is the solute's diffusion coefficient in water (approximately $5 \times 10^{-10}\,\mathrm{m^2\,s^{-1}}$ for sucrose at physiological concentrations), and a is the cross-sectional area of the tube. Using data from Fig. 3 for all z and t, we find that the diffusion term is at all times at least five orders of magnitude smaller than the convective term. Hence, diffusive solute flux is negligible relative to convective flux, and the second term on the right of eqn (C.1) drops out to give eqn (4).

While axial diffusion is slow relative to convection, it turns out that it is sufficiently fast to ensure a radially homogeneous distribution of solute. Following Taylor (1954), if

$$\frac{r^2 v}{4D_m L} \ll 1, \tag{C.2}$$

where L is the length over which solute concentrations undergo a significant change, and is defined such that $(1/L)$ equals the mean value of $(1/c)(\partial c/\partial z)$ over the experimental (or model) domain, then the time-scale of radial diffusion is far less than the time required for the solution to move axially into a region where the concentration changes appreciably. From Fig. 3 at $t = 24\,\mathrm{hr}$, we find an appropriate value of L to be $\sim 6\,\mathrm{m}$, and using that value, and the very highest transport velocities v mentioned in the phloem literature ($\sim 300\,\mathrm{cm\,hr^{-1}}$, Passioura & Ashford, 1974), the condition in eqn (C.2) is satisfied by more than six orders of magnitude. Rapid radial diffusion indicates the possibility of strong Taylor dispersion, but we find that the dispersion coefficient is of the same order as diffusion—i.e. $rv/D_m \approx 10$ (Taylor, 1954)—and as axial diffusion is negligible, we can similarly discount axial dispersion.

Appendix D

Modified Newton–Raphson Method

The time-stepping method used in this work is called the "modified Newton–Raphson" technique (Istok, 1989; called "modified-Picard" by Celia *et al.*, 1990), which uses past estimates of the solution to solve not for new estimates, but for corrections or increments to those estimates. The correction to some state factor X is added to the initial estimate of X in the following way:

$$X^{m+1} = X^m + \delta X^m, \tag{D.1}$$

where δX^m is the correction to X between iteration m and iteration $m+1$.

The change in the state of the system between time steps n and $n+1$ is given by

$$\Delta X^{n+1} = X^{n+1} - X^n, \tag{D.2}$$

where ΔX^{n+1} is the backwards-difference (or fully implicit) time step increment. This can be rewritten to account for the iteration number m as

$$\Delta X^{n+1,\,m+1} = X^{n+1,\,m+1} - X^n, \tag{D.3}$$

where the change in X between the current time step and the last is defined at the $(n+1)$st time step and $(m+1)$st iteration, and this can be expanded to read:

$$\Delta X^{n+1,\,m+1} = (X^{n+1,\,m+1} - X^{n+1,\,m}) + X^{n+1,\,m} - X^n, \tag{D.4}$$

where the quantity in the parentheses is the difference in state across an iteration. Equation (D.4) is the fully expanded modified Newton–Raphson iteration equation. The change in state between iterations, or, otherwise stated, the correction to the previous estimate of the change in state between time steps, can now be rewritten as

$$\delta X^m = X^{n+1,\,m+1} - X^{n+1,\,m}, \tag{D.5}$$

where upon insertion into eqn (D.4) and some rearrangement we find:

$$X^{n+1,\,m+1} = X^{n+1,\,m} + \delta X^m. \tag{D.6}$$

During every time step, $X^{n+1,m+1}$ in eqn (D.6) is decomposed for each iteration into what is known ($X^{n+1,\,m}$) and what is unknown (δX^m). This method dramatically improves the stability of the numerical simulation. Note that discretized variables are written with capital letters.

D.1. DISCRETIZATION OF TIME DERIVATIVES

The following sections show the discretization of each of the derivatives in eqns (16) and (17). Following Celia *et al.* (1990), using a truncated Taylor series expansion, the time derivative for volume conservation is given by

$$\frac{\partial}{\partial t}(A_i^{n+1,m+1}) \approx \frac{A_i^{n+1,m} - A_i^n}{\Delta t} + \frac{A_i^{n+1,m}}{\varepsilon \Delta t}\delta P_i^m, \quad \text{(D.7)}$$

whereas the time derivative for sucrose conservation is given by

$$\begin{aligned}\frac{\partial}{\partial t}[C_i^{n+1,\,m+1} A_i^{n+1,\,m+1}] &\approx \frac{C_i^{n+1,\,m} A_i^{n+1,\,m+1} - C_i^n A_i^n}{\Delta t} \\ &+ \frac{A_i^{n+1,\,m+1}}{\Delta t}\delta C_i^m. \end{aligned} \quad \text{(D.8)}$$

D.2. PASSIVE WATER FLUX ACROSS PLASMA MEMBRANE

The equation for passive membrane water flux is given by

$$\begin{aligned}W_i^{n+1,\,m+1} = D_i^{n+1,\,m}[\Psi_i^o - (P_i^{n+1,\,m} + \Psi_{\pi,i}^{n+1,\,m}) \\ - (\delta P_i^m + \delta \Psi_{\pi,i}^m)], \end{aligned} \quad \text{(D.9)}$$

where

$$D_i^{n+1,\,m} = 2\pi R_i^{n+1,\,m} L_p, \quad \text{(D.10)}$$

and δP_i^m and $\delta \Psi_{\pi,i}^m$ are both unknowns. Note that $\delta \Psi_{\pi,i}^m$ can be written in terms of δC_i^m if we let

$$\delta \Psi_{\pi,i}^m = \left.\frac{\mathrm{d}\psi_\pi}{\mathrm{d}c}\right|_i^{n+1,\,m} \delta C_i^m = G_i^{n+1,\,m}\delta C_i^m. \quad \text{(D.11)}$$

For now, we let

$$Q_i^{n+1,\,m} \approx \delta C_i^m, \quad \text{(D.12)}$$

where $Q_i^{n+1,\,m}$ is an *estimate* of the change in solute concentration, but actually a function of δP_i^m, the derivation of which will be described later. Equation (D.9) is now written in terms of δP_i^m:

$$\begin{aligned}W_i^{n+1,\,m+1} = D_i^{n+1,\,m}[\Psi_i^o - P_i^{n+1,\,m} - \Psi_{\pi,i}^{n+1,\,m} \\ - G_i^{n+1,\,m} Q_i^{n+1,\,m}] \\ - D_i^{n+1,\,m}\delta P_i^m, \end{aligned} \quad \text{(D.13)}$$

where $G_i^{n+1,\,m}$ is solely a function of sucrose concentration and temperature, and is given by

$$G = \frac{\mathrm{d}\psi_\pi}{\mathrm{d}c} = -\frac{\Re T(0.998 + 0.178\,m)}{(1 - \overline{V_s}c)^2}. \quad \text{(D.14)}$$

D.3. AXIAL FLOW OF SIEVE TUBE SAP

The divergence in flow in the volume conservation equation is given by

$$\frac{\partial}{\partial z}(J_i^{n+1,m+1}) \approx S_i^{n+1,m} + \frac{\delta J_{i,+}^m - \delta J_{i,-}^m}{\Delta z}, \quad \text{(D.15)}$$

where

$$S_i^{n+1,\,m} = \frac{J_{i,+}^{n+1,\,m} - J_{i,-}^{n+1,\,m}}{\Delta z}, \quad \text{(D.16)}$$

and $J_{i,+}$ ($\mathrm{m^3\,s^{-1}}$) is the flux between the i-th node and the $(i+1)$-th node, defined positive in the positive-z direction, and $J_{i,-}$ is the flux between the $(i-1)$-th and ith node, again defined positive in the positive-z direction. $J_{i,+}^{n+1,\,m}$ and $J_{i,-}^{n+1,\,m}$ are given by:

$$\begin{aligned}J_{i,+}^{n+1,\,m} &= -k_{i,+}^{n+1,\,m}\frac{P_{i+1}^{n+1,\,m} - P_i^{n+1,\,m}}{\Delta z}, \\ J_{i,-}^{n+1,\,m} &= -k_{i,-}^{n+1,\,m}\frac{P_i^{n+1,\,m} - P_{i-1}^{n+1,\,m}}{\Delta z}. \end{aligned} \quad \text{(D.17)}$$

Subsuming Δz into k, we get

$$\begin{aligned}J_{i,+}^{n+1,\,m} &= -K_{i,+}^{n+1,\,m}(P_{i+1}^{n+1,\,m} - P_i^{n+1,\,m}), \\ J_{i,-}^{n+1,\,m} &= -K_{i,-}^{n+1,\,m}(P_i^{n+1,\,m} - P_{i-1}^{n+1,\,m}), \end{aligned} \quad \text{(D.18)}$$

where is K ($\mathrm{m^3\,s^{-1}\,MPa^{-1}}$) is the *conductance* of the sieve tube section, rather than the *conductivity* k. K is calculated for each node separately

using a discrete version of our sieve-plate-modified Hagen–Poiseuille relation

$$K_i^{n+1,\,m} = \beta \frac{\pi (R_i^{n+1,\,m})^4}{8\mu_i^{n+1,\,m}\Delta z}. \tag{D.19}$$

$K_{i,+}^{n+1,\,m}$ and $K_{i,-}^{n+1,\,m}$ are given by the harmonic means of the K's of the bounding nodes. Following eqn (D.18) for δJ^m, we can write a simplified version of eqn (D.15):

$$\frac{\partial}{\partial z}(J_i^{n+1,\,m+1}) \approx S_i^{n+1,\,m} + H_i^{n+1,\,m}\delta P_i^m - H_{i,+}^{n+1,\,m}\delta P_{i+1}^m - H_{i,-}^{n+1,\,m}\delta P_{i-1}^m, \tag{D.20}$$

where H is given by

$$H_{i,+}^{n+1,\,m} = \frac{K_{i,+}^{n+1,\,m}}{\Delta z},$$
$$H_{i,-}^{n+1,\,m} = \frac{K_{i,-}^{n+1,\,m}}{\Delta z},$$
$$H_i^{n+1,\,m} = H_{i,+}^{n+1,\,m} + H_{i,-}^{n+1,\,m}. \tag{D.21}$$

The divergence in solute flow in the sucrose conservation equation must be dealt with slightly differently. It is given by

$$\frac{\partial}{\partial z}(C_i^{n+1,\,m+1} J_i^{n+1,\,m+1}) \approx \frac{C_{i,+}^{n+1,\,m+1} J_{i,+}^{n+1,\,m+1} - C_{i,-}^{n+1,\,m+1} J_{i,-}^{n+1,\,m+1}}{\Delta z}, \tag{D.22}$$

where $C_{i,+}^{n+1,m+1}$ is the effective sucrose concentration for flow from node i to node $i+1$, and $C_{i,-}^{n+1,m+1}$ from node $i-1$ to node i. Simulations of solute convection can be very sensitive to the way the intermediate solute concentrations are calculated. If those values are set too low heading into a "shock zone", where for instance axial solute flow is rapid into a region where there is little solute, large spatial oscillations can develop. If they are set too high, the concentration front is smeared. The method of characteristics, which casts the convection term in a Lagrangian reference frame, has been proposed to deal with some of these difficulties (Ewing & Wang, 2001), but we have chosen to use a slope-limiting total variation diminishing (TVD) method, which is more appropriate under the Eulerian scheme employed here (Goodman & LeVeque, 1988), and simpler to implement. Under this scheme, the concentration profile is broken up into a series of piecewise linear segments with mean value equal to the concentration at that node and slope determined by the following:

$$\dot{C}_i = \frac{\partial}{\partial z}(C_i) = \text{minmod}\left\{\frac{C_{i+1} - C_i}{\Delta z}, \frac{C_i - C_{i-1}}{\Delta z}\right\}, \tag{D.23}$$

where $\text{minmod}(a,b) = 1/2(\text{sgn}(a) + \text{sgn}(b))\min(|a|,|b|)$. Once these slopes are calculated, the direction of flow is determined, and the concentration at the node boundary is calculated as a logical linear combination of the slopes from eqn (D.23), such that

$$C_{i,+} = \{J_{i,+} > 0\}\left(C_{i+1} + \frac{2}{\Delta z}\dot{C}_{i+1}\right) + \{J_{i,+} < 0\}\left(C_i - \frac{2}{\Delta z}\dot{C}_i\right)$$
$$C_{i,-} = \{J_{i,-} > 0\}\left(C_i + \frac{2}{\Delta z}\dot{C}_i\right) + \{J_{i,-} < 0\}\left(C_{i-1} - \frac{2}{\Delta z}\dot{C}_{i-1}\right), \tag{D.24}$$

where the expressions in curly brackets are evaluated as 1 if true and 0 if false for each node i. These definitions ensure that solute is properly distributed in "shock zones". Spatial oscillations are eliminated, but some solute smearing is observed at low spatial and temporal resolutions. This is the first numerical model of solute advection in the phloem to use such a scheme.

The complicated nature of these definitions precludes extracting a δC_i^m term from eqn (D.24) as in eqn (D.6). However, it is apparently sufficient to ignore that problem and rewrite eqn (D.22) as

$$\frac{\partial}{\partial z}(C_i^{n+1,\,m+1} J_i^{n+1,\,m+1}) \approx \frac{C_{i,+}^{n+1,\,m} J_{i,+}^{n+1,\,m+1} - C_{i,-}^{n+1,\,m} J_{i,-}^{n+1,\,m+1}}{\Delta z}, \tag{D.25}$$

where $C_{i,+}^{n+1,m}$ and $C_{i,-}^{n+1,m}$ are defined according to eqn (D.24) using flow rates estimated for the $(n+1,m)$-th iteration.

D.4. CONSTRUCTION OF DISCRETE VOLUME CONSERVATION EQUATION

We can now construct a complete, discretely defined version of the volume conservation equation:

$$\begin{aligned}&\frac{A_i^{n+1,m}-A_i^n}{\Delta t}+\frac{A_i^{n+1,m}}{\varepsilon\Delta t}\delta P_i^m\\&\quad=D_i^{n+1,m}[\Psi_i^o-P_i^{n+1,m}-\Psi_{\pi,i}^{n+1,m}\\&\quad-G_i^{n+1,m}Q_i^{n+1,m}]-D_i^{n+1,m}\delta P_i^m+\overline{V_s}B_i^{n+1,m+1}\\&\quad-S_i^{n+1,m}-H_i^{n+1,m}\delta P_i^m\\&\quad+H_{i,+}^{n+1,m}\delta P_{i+1}^m+H_{i,-}^{n+1,m}\delta P_{i-1}^m,\end{aligned}\tag{D.26}$$

noting that $Q_i^{n+1,m}$ has yet to be derived and depends on P. From this we obtain

$$\begin{aligned}&\left[\frac{A_i^{n+1,m}}{\varepsilon\Delta t}+D_i^{n+1,m}+H_i^{n+1,m}\right]\delta P_i^m\\&\quad+[-H_{i,+}^{n+1,m}]\delta P_{i+1}^m+[-H_{i,-}^{n+1,m}]\delta P_{i-1}^m\\&=-\left[\frac{A_i^{n+1,m}-A_i^n}{\Delta t}\right]\\&\quad+D_i^{n+1,m}[\Psi_i^o-P_i^{n+1,m}-\Psi_{\pi,i}^{n+1,m}\\&\quad-G_i^{n+1,m}Q_i^{n+1,m}]+\overline{V_s}B_i^{n+1,m+1}-S_i^{n+1,m},\end{aligned}\tag{D.27}$$

which is solved for δP_i^m. Pressure, flow and cross-sectional area estimates are revised, and then used to solve for the concentration correction, δC_i^m, as shown below.

D.5. CONSTRUCTION OF DISCRETE SUCROSE CONSERVATION EQUATION

The discrete version of the sucrose conservation equation follows on that of the volume conservation equation:

$$\begin{aligned}&\frac{C_i^{n+1,m}A_i^{n+1,m+1}-C_i^nA_i^n}{\Delta t}+\frac{A_i^{n+1,m+1}}{\Delta t}\delta C_i^m\\&=B_i^{n+1,m+1}\\&\quad-\frac{C_{i,+}^{n+1,m}J_{i,+}^{n+1,m+1}-C_{i,-}^{n+1,m}J_{i,-}^{n+1,m+1}}{\Delta z},\end{aligned}\tag{D.28}$$

from which we obtain

$$\begin{aligned}\delta C_i^m=&\frac{\Delta t}{A_i^{n+1,m+1}}B_i^{n+1,m+1}\\&-\frac{C_i^{n+1,m}A_i^{n+1,m+1}-C_i^nA_i^n}{A_i^{n+1,m+1}}\\&-\Delta t\frac{C_{i,+}^{n+1,m}J_{i,+}^{n+1,m+1}-C_{i,-}^{n+1,m}J_{i,-}^{n+1,m+1}}{A_i^{n+1,m+1}\Delta z}.\end{aligned}\tag{D.29}$$

δC_i^m is used to revise estimates of concentration, viscosity and solute potential for use in the next iteration.

D.6. ESTIMATE OF Q FOR VOLUME CONSERVATION EQUATION

$Q_i^{n+1,m}$ could be left out of eqn (D.27) (i.e. set equal to zero), but its inclusion dramatically increases the stability of the model at low spatial and temporal resolution. In essence, $Q_i^{n+1,m}$ provides a highly accurate estimate of δC_i^m without actually solving the solute conservation equation. To solve for $Q_i^{n+1,m}$, we must discretize the sucrose flow divergence term in terms of P rather than C, so that C is in terms of iteration $(n+1,m)$ rather than iteration $(n+1,m+1)$, and δJ_i^m is in terms of δP_i^m:

$$\begin{aligned}&\frac{\partial}{\partial z}(C_i^{n+1,m}J_i^{n+1,m+1})\\&\quad\approx\frac{C_{i,+}^{n+1,m}J_{i,+}^{n+1,m}-C_{i,-}^{n+1,m}J_{i,-}^{n+1,m}}{\Delta z}\\&\quad+[C_{i,+}^{n+1,m}H_{i,+}^{n+1,m}+C_{i,-}^{n+1,m}H_{i,-}^{n+1,m}]\delta P_i^m\\&\quad-[C_{i,+}^{n+1,m}H_{i,+}^{n+1,m}]\delta P_{i+1}^m-[C_{i,-}^{n+1,m}H_{i,-}^{n+1,m}]\delta P_{i-1}^m,\end{aligned}\tag{D.30}$$

where H is defined according to eqn (D.21).

The time derivative is written in terms of δC_i^m, following eqn (D.8), and is denoted as $Q_i^{n+1,m}$:

$$\begin{aligned}&\frac{\partial}{\partial t}[C_i^{n+1,m+1}A_i^{n+1,m}]\\&\quad\approx\frac{C_i^{n+1,m}A_i^{n+1,m}-C_i^nA_i^n}{\Delta t}+\frac{A_i^{n+1,m}}{\Delta t}Q_i^{n+1,m}.\end{aligned}\tag{D.31}$$

Now, rewriting the solute conservation equation using eqns (D.30) and (D.31), we can solve for $Q_i^{n+1,m}$:

$$Q_i^{n+1,m} = U_i^{n+1,m} - F_i^{n+1,m}\delta P_i^m + F_{i,+}^{n+1,m}\delta P_{i+1}^m + F_{i,-}^{n+1,m}\delta P_{i-1}^m, \quad \text{(D.32)}$$

where

$$F_{i,+}^{n+1,m} = \frac{\Delta t}{A_i^{n+1,m}}[C_{i,+}^{n+1,m} H_{i,+}^{n+1,m}],$$

$$F_{i,-}^{n+1,m} = \frac{\Delta t}{A_i^{n+1,m}}[C_{i,-}^{n+1,m} H_{i,-}^{n+1,m}],$$

$$F_i^{n+1,m} = F_{i,+}^{n+1,m} + F_{i,-}^{n+1,m},$$

$$U_i^{n+1,m} = \frac{\Delta t}{A_i^{n+1,m}} B_i^{n+1,m}, - \left[\frac{C_i^{n+1,m} A_i^{n+1,m} - C_i^n A_i^n}{A_i^{n+1,m}}\right] - \frac{\Delta t}{A_i^{n+1,m}}\left[\frac{C_{i,+}^{n+1,m} J_{i,+}^{n+1,m} - C_{i,-}^{n+1,m} J_{i,-}^{n+1,m}}{\Delta z}\right], \quad \text{(D.33)}$$

to obtain from eqn (D.27):

$$\left[\frac{A_i^{n+1,m}}{\varepsilon \Delta t} + D_i^{n+1,m} - D_i^{n+1,m} G_i^{n+1,m} F_i^{n+1,m} + H_i^{n+1,m}\right]\delta P_i^m + [D_i^{n+1,m} G_i^{n+1,m} F_{i,+}^{n+1,m} - H_{i,+}^{n+1,m}]\delta P_{i+1}^m + [D_i^{n+1,m} G_i^{n+1,m} F_{i,-}^{n+1,m} - H_{i,-}^{n+1,m}]\delta P_{i-1}^m = -\left[\frac{A_i^{n+1,m} - A_i^n}{\Delta t}\right] + D_i^{n+1,m} [\Psi_i^o - P_i^{n+1,m} - \Psi_{\pi,i}^{n+1,m} - G_i^{n+1,m} U_i^{n+1,m}] + \overline{V_s} B_i^{n+1,m} - S_i^{n+1,m}. \quad \text{(D.34)}$$

This is the version of the volume conservation equation used to calculate δP_i^m.

Appendix E

Mass Balance and Convergence

At the end of every iteration, the model domain is checked for global mass balance (i.e. the gross flux of material into the model domain must equal the change in the quantity of material in the domain plus the gross flux out to within a certain error tolerance). If mass balance is satisfied, then the model terminates the time step with that iteration and continues to the next time step. Here, mass balance errors are as small as the floating point precision of the processor, but an arbitrary error tolerance of 10^{-8} was set to save time.

The degree of convergence on steady state can be found far in advance of its actually occurring given the fact that the system approaches steady state in a logarithmic manner. At each time step, the pressure and sucrose concentration states of the system are given as

$$\theta_{PV} = \sum_i^N P_i^{n+1,m} V_i^{n+1,m},$$

$$\theta_{CV} = \sum_i^N C_i^{n+1,m} V_i^{n+1,m}, \quad \text{(E.1)}$$

where θ_{PV} is the total pressure-volume energy (MPa m^3 = MJ) of the model domain, and θ_{CV} is the total sucrose content (mol). The steady-state convergence χ (dimensionless) with respect to either pressure–volume or sucrose content is then given by

$$\chi = \frac{-\dot{\theta}^2}{\theta\ddot{\theta} - \dot{\theta}^2}, \quad \text{(E.2)}$$

where $\dot{\theta}$ is the first derivative of θ with time (for either pressure or concentration), and $\ddot{\theta}$ is the second derivative. A value of 10^{-4} for χ indicates that the model has converged to within 1/100 of a percent of steady state.

The time rate of change in θ is log-linear:

$$\ln(\dot{\theta}) = \sigma t + \gamma, \quad \text{(E.3)}$$

where σ is slope of the line (when $\sigma < 0$) and γ is its y-intercept. Taking the exponents of both sides, we find

$$\dot{\theta} = e^{\sigma t + \gamma}, \quad \text{(E.4)}$$

whereas the derivative of both sides of eqn (E.3) is given by

$$\frac{\ddot{\theta}}{\dot{\theta}} = \sigma. \quad \text{(E.5)}$$

Integration of eqn (E.4) gives

$$\theta = \frac{1}{\sigma} e^{\sigma t+\gamma} + \theta_o, \tag{E.6}$$

where θ_o is the state of the model domain at steady state.

We wish to know the closeness of the current state θ to the steady state θ_o, χ:

$$\chi = \frac{\theta_o - \theta}{\theta_o}. \tag{E.7}$$

Solving eqn (E.6) for θ_o and inserting into eqn (E.7) we find

$$\chi = \frac{-e^{\sigma t+\gamma}}{\sigma\theta - e^{\sigma t+\gamma}}, \tag{E.8}$$

or, by eqns (E.4) and (E.5):

$$\chi = \frac{-\dot{\theta}^2}{\theta\ddot{\theta} - \dot{\theta}^2}. \tag{E.9}$$

This estimate of χ can be used only when $\dot{\theta}$ is log-linear with a negative slope.

To test the conservation and convergence characteristics of the model, we ran a 7 day simulation at $f = 20\,\text{nodes}\,\text{m}^{-1}$ and $\Delta t = 10.0\,\text{s}$, with $c(z, t = 0)$ and $p(z, t = 0)$ both set equal to zero. The mass balance of both volume and sucrose content [Fig. E1(A)] can be maintained at well less than the required 10^{-8} precision throughout the simulation, and, as the simulation progresses, this criterion becomes increasingly easy to meet [Fig. E1(B)]. Sucrose mass balance is superior to volume conservation because of the sucrose conservation equation's linearity. The pressure and concentration convergence estimates χ are shown in Figs. E1(C) and (D), as is the rate of change in these quantities, which varies log-linearly with time.

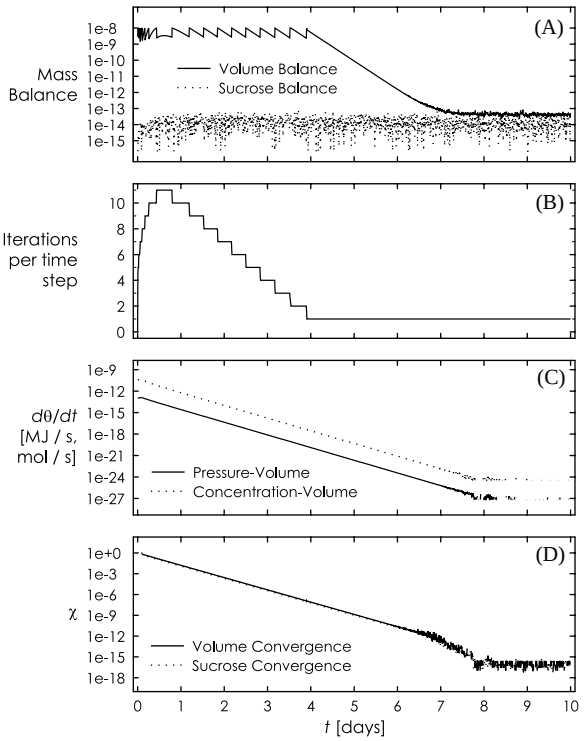

FIG. E1. The conservation and convergence characteristics of a 10 day simulation of an idealized sieve tube of length $L = 5\,\text{m}$ performed at a relatively low spatial resolution $f = 20\,\text{nodes}\,\text{m}^{-1}$, and a time step length of $\Delta t = 10\,\text{s}$, as described in Appendix E. All other parameters are as in the legend to Fig. 3. (A) A semilog plot of the conservation of volume and sucrose. Sucrose conservation is always excellent (due to the linearity of the sucrose conservation equation), while volume conservation becomes the limiting factor in determining the number of iterations necessary for convergence during each time step. Here, we require that both volume and sucrose conservation be maintained to within 10^{-8}. (B) The number of iterations required to meet the 10^{-8} conservation criterion during each time step. As the simulation approaches steady state, a decreasing number of iterations are required to meet this criterion. (C) The rate of change in the pressure and concentration states of the system with time. This function must be log-linear—and it is—in order to use the convergence estimate described in eqn (E.9). (D) Convergence on steady state, given by the dimensionless quantity χ, represents the fractional distance from steady state, calculated using eqn (E.9). The calculation of χ breaks down after 6.5 days when the temporal change in pressure and concentration nears the floating-point precision of the computer.

Appendix F

Model Resolution

Near-perfect mass balance is achieved in this simulation irrespective of temporal or spatial resolution. However, a drop in resolution can lead to changes in the solute profile in ways that are not necessarily physical. As mentioned above, to prevent spatial oscillations in "shock zones" it is necessary to alter the concentration at the boundary between nodes so that it is higher than the mean value, thus preventing solute from "backing up" in the upstream node (Ewing & Wang, 2001). However, one consequence of this correction is that slightly more

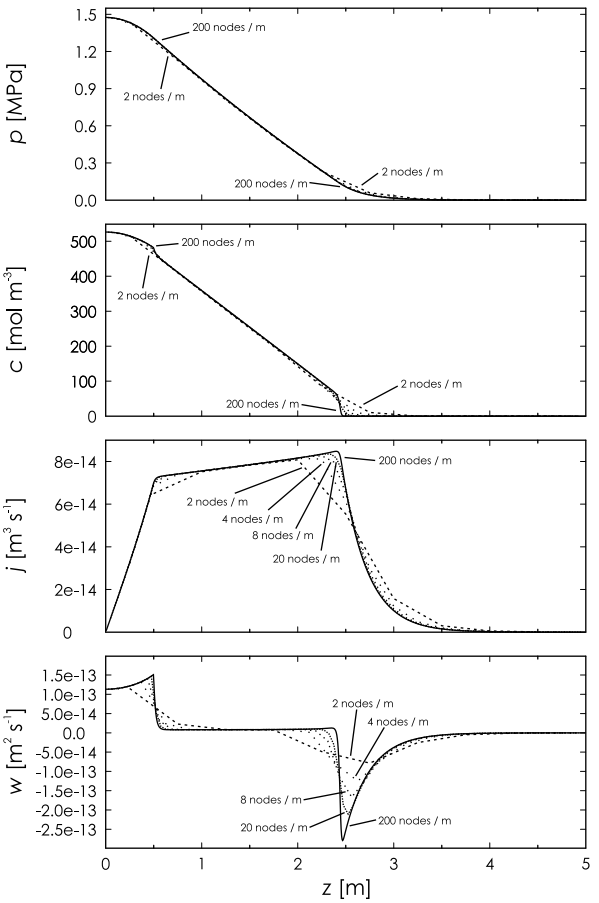

FIG. F1. Pressure p, concentration c, axial volume flux j, and membrane water flux w at 1 hr into a set of 24 hr simulations performed at one temporal resolution ($\Delta t = 1$ s) and several spatial resolutions ($f = 2$, 4, 8, 20, and 200 nodes m^{-1}) in an idealized sieve tube of length $L = 5$ m, as described in Appendix F.1. All other parameters are as described in the legend to Fig. 3.

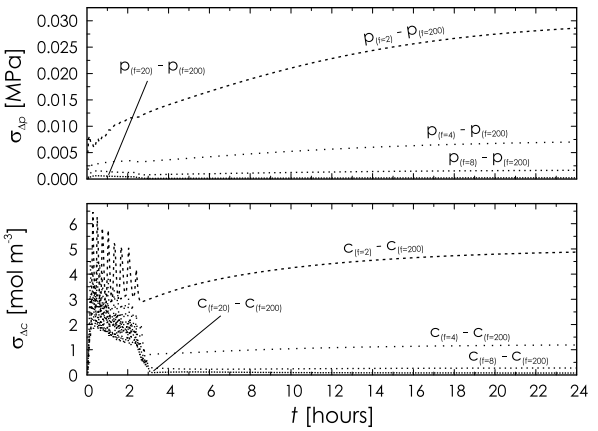

FIG. F2. The standard deviations of the profiles of pressure and concentration between each of the lower spatial resolution simulations ($f = 2$, 4, 8, and 20 nodes m^{-1}) and the high spatial resolution simulation ($f = 200$ nodes m^{-1}) at $\Delta t = 1$ s. These data are from the same simulations as in Fig. F1, described in Appendix F.1. The standard deviations are highest early in the simulations and decline after 3 hr, as the concentration front reaches the far end of the sieve tube. The early noisy differences between the concentration profiles of the different simulations is a local effect of the slope-limiting total variation diminishing (TVD) method applied to the front, as used in this work. It does not reflect significant changes in the concentration profile, just a phase shift between those variations among simulations of different spatial resolution.

solute is transported through the "shock zones" than is actually merited by the solution velocity at low spatial or temporal resolution. This effect is called "solute smearing".

Another problem that occurs at low resolution is due to the discrete nature of the model domain. As solute flows from one node to the next, that solute is immediately distributed evenly throughout the downstream node, irrespective of its length, smearing the concentration front. When Δt or Δz is large, the effect, called "numerical diffusion" (Fried, 1975), is to add a diffusion term to the solute conservation equation. Both solute smearing and numerical diffusion disappear at high temporal and spatial resolutions.

The simulation is robust to Courant numbers Cr of up to 0.4, where Cr is given by:

$$Cr = v\frac{\Delta t}{\Delta z}, \tag{F.1}$$

and improves as Cr becomes very small. In the following sections, we address the minimum spatial and temporal resolution necessary to limit the strength of solute smearing and numerical diffusion under non-steady-state and steady-state conditions, for a 5 m sieve tube, whose parameter values are identical to those described in Section 3.1.

F.1. SPATIAL RESOLUTION

Five 24 hr (86 400 s) simulations of a 5 m sieve tube were performed at $\Delta t = 1.0$ s and $f = 200$, 20, 8, 4, or 2 nodes m^{-1}. Figure F1 shows the state of pressure, concentration, axial flux, and membrane water flux of these simulations at $t = 3600$ s (1 hr). Irrespective of spatial resolution, the major features of the simulations agree,

except at low resolution where the concentration front is smeared relative to simulations run at higher resolutions. This, of course, has its effect on pressure, membrane water flux, and axial velocity, as well. However, at high resolution, the concentration front is extremely sharp, whereas when f drops below $20\,\text{nodes}\,\text{m}^{-1}$, the front is largely gone. We attributed the divergence among simulations to be largely the result of increased solute smearing at lower resolutions.

The standard deviation of the differences in concentration and pressure between lower resolution simulations and the $f = 200\,\text{nodes}\,\text{m}^{-1}$ simulation were calculated for each (Fig. F2). For pressure, low-resolution simulations deviate from the high-resolution simulation only minimally at first, increasing later as the system approaches steady state. This increase is due to solute smearing at low resolution, which causes excess sucrose to be removed from the system via the unloading zone than would otherwise be at higher resolution. In fact, the total sucrose content of the system increases more slowly on approach to steady state for low-resolution simulations that it does for high-resolution simulations. This is borne out in the standard deviations in sucrose concentration between the simulations, where, following an initial state of high variability prior to $t = 3\,\text{hr}$, which will be explained shortly, the deviation between simulations also increases with time.

After $t = 3\,\text{hr}$, the sucrose front has arrived at the far end of the tube. But prior to that, the concentration front is its own moving "shock zone", and the slope-limiting total variation diminishing (TVD) method used here introduces some temporal variation at the front in the rate at which solutes are allowed to pass from one node to the next. This variation occurs at different frequencies at different spatial resolutions, proportionally to the front velocity divided by the node spacing. The effect is to produce oscillations in the standard deviation of

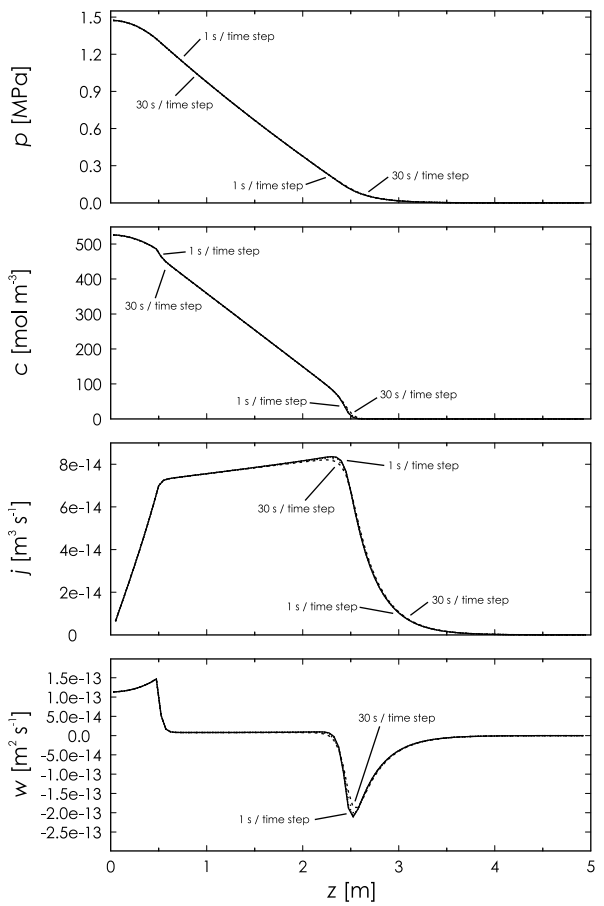

FIG. F3. Pressure p, concentration c, axial volume flux j, and membrane water flux w at 1 hr into a set of 24 hr simulations performed at one spatial resolution ($f = 20\,\text{nodes}\,\text{m}^{-1}$) and several temporal resolutions ($\Delta t = 1$, 3, 6, 15, and 30 s) in an idealized sieve tube of length $L = 5\,\text{m}$, as described in Appendix F.2. All other parameters are as described in the legend to Fig. 3.

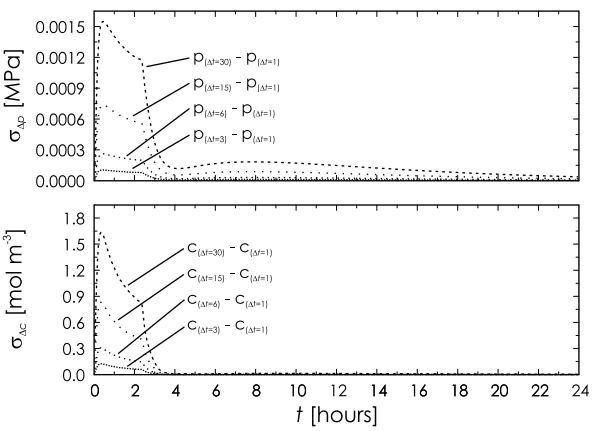

FIG. F4. The standard deviations of the profiles of pressure and concentration between each of the lower temporal resolution simulations ($\Delta t = 3$, 6, 15, and 30 s) and the high temporal resolution simulation ($\Delta t = 1\,\text{s}$) at $f = 20\,\text{nodes}\,\text{m}^{-1}$. These data are from the same simulations as Fig. F3, as described in Appendix F.2. The standard deviations are highest early in the simulation and decline after 3 hr, as the concentration front reaches the far end of the sieve tube. Thereafter, the differences become vanishingly small.

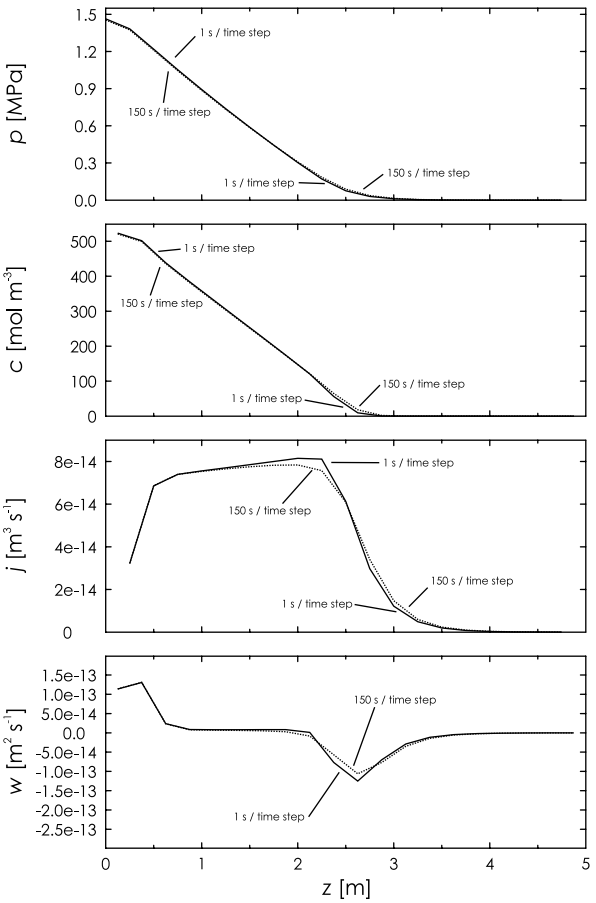

FIG. F5. Pressure p, concentration c, axial volume flux j, and membrane water flux w at 1 hr into a set of 24 hr simulations performed at one spatial resolution ($f = 4$ nodes m^{-1}) and several temporal resolutions ($\Delta t = 1$, 5, 25, 50, 75, and 150 s) in an idealized sieve tube of length $L = 5$ m, as described in Appendix F.2. Only data for $\Delta t = 1$, 150 s are shown. All other parameters are as described in the legend to Fig. 3.

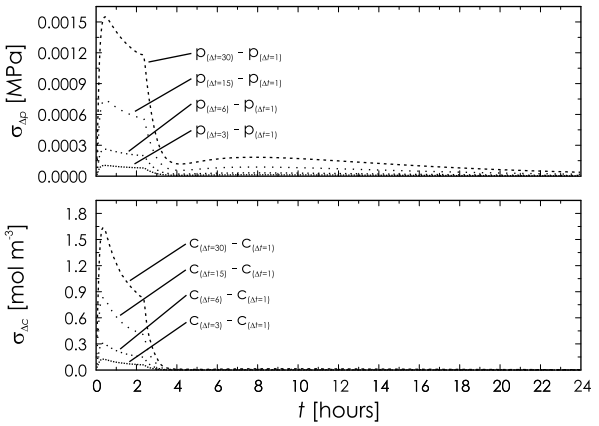

FIG. F6. The standard deviations of the profiles of pressure and concentration between each of the lower temporal resolution simulations ($\Delta t = 5$, 25, 50, 75, and 150 s) and the high temporal resolution simulation ($\Delta t = 1$ s) at $f = 4$ nodes m^{-1}. These data are from the same simulations as Fig. F5, as described in Appendix F.2. The standard deviations are highest early in the simulation and decline after 3 hr, as the concentration front reaches the far end of the sieve tube. After this point, the differences become vanishingly small.

concentration between the low- and high-resolution simulations. In fact, though we performed these simulations at a 1 s time step, we sampled the data from the simulation every 150 s and the oscillations seen in the figure are aliased versions of the noise actually produced between the simulations. It should be noted that this does *not* mean that the TVD method introduces noise into the calculation itself (as can be seen in Fig. 3), but rather that it handles sucrose flow across the front in quantitatively slightly different ways depending on the spatial resolution. It would seem from Fig. F1 that simulations performed at $f = 4$ nodes m^{-1} or better, though lacking in the fine spatial detail afforded by the high-resolution simulation, will provide the same qualitative information as the higher-resolution simulation.

F.2. TEMPORAL RESOLUTION

To test the effect of drops in temporal resolution a series of five 24 hr (86 400 s) simulations of a 5 m sieve tube were performed at $f = 20$ nodes m^{-1} and $\Delta t = 1.0$, 3.0, 6.0, 15.0, and 30.0 s (Figs F3 and F4; temporal resolutions worse than $\Delta t = 30.0$ s result in $Cr > 0.4$), as well as another six 24 hr simulations at $f = 4$ nodes m^{-1} and $\Delta t = 1.0$, 5.0, 25.0, 50.0, 75.0, and 150.0 s (Figs F5 and F6; temporal resolutions worse than $\Delta t = 150.0$ s result in $Cr > 0.4$).

We find that the numerical solution is exceedingly robust to changes in temporal resolution. Figure F3 shows a comparison for p, c, j, and w, as in Fig. F1, of the same simulation at $f = 20$ nodes m^{-1} but at different time step lengths, and at $t = 1$ hr. Very little difference can be observed between them, and what difference is present is stereotypically that of numerical diffusion, which becomes stronger at low temporal resolutions (or high Cr). Figure F4 shows profile-wide standard deviations for all t

from $t = 0$ to $t = 24$ hr. Before the sucrose front reaches the far end of the tube at $t = 3$ hr, the error is somewhat higher than it is after, where the differences between simulations becomes vanishingly small. The same can be said at an even lower spatial resolutions ($f = 4$ nodes m^{-1}), where differences are due to numerical diffusion at large values of Cr (Fig. F5), and become vanishingly small once the sucrose front has reached the far end of the sieve tube (Fig. F6). It should also be noted that the errors due to differences in temporal resolution appear to be linearly proportional to the ratios of time step lengths (Figs F4 and F6).

The numerical solution presented here appears to be quite robust at any temporal resolution (provide the Courant number Cr does not exceed approximately 0.4). Spatial resolution is far more critical, especially if the user is need of accurately shaped concentration profiles, and also critical for minimizing solute smearing around the points where the gradient in concentration is changing rapidly (i.e. near rapidly moving sucrose fronts).